# UNIVERSITÀ DEGLI STUDI DI NAPOLI "FEDERICO II"

DOTTORATO DI RICERCA
IN
TERAPIE AVANZATE MEDICO-CHIRURGICHE
XXIX CICLO

Tesi Sperimentale di Dottorato

# Association of FGFR1 with ERα maintains ligand-independent ER transcription and mediates resistance to estrogen deprivation in breast cancer

RELATORE
Chiar.mo/a
Prof. Sabino De Placido

CANDIDATO
Dott. Luigi Formisano

## INTRODUCTION

Amplification of the chromosomal region 8p11-12, the genomic location of fibroblast growth factor receptor 1 (*FGFR1),* has been reported in breast, ovarian, bladder, lung and oral squamous cancers, and in rhabdomyosarcoma (1-7). *FGFR1* amplification occurs in ~10% of patients with ER+/HER2-negative breast cancer where it is associated with early relapse following adjuvant tamoxifen therapy and with poor survival (8). Blockade of FGFR1 signalling by pharmacological or genetic approaches in human breast cancer cells harboring *FGFR1* amplification leads to decreased cell growth and survival, suggesting *FGFR1* gene amplification is a surrogate of cancer cell dependence on aberrant FGFR activity (8).

FGFRs belong to the family of receptor tyrosine kinases (RTKs) that consist of an extracellular ligand-binding domain linked to an intracellular catalytic protein kinase core via a single-pass transmembrane domain (TMD) (9). Binding of FGF ligands induces receptor dimerization, activation of the kinase domain and phosphorylation of C-terminal tyrosines to which adaptor proteins dock, followed by activation of signal transduction pathways, including PI3K/AKT, RAS/RAF/MEK/ERK, phospholipase Cγ (PLCγ) and STATs (10). In addition, there is strong evidence that FGFRs traffic to the nucleus, where they may function in a different manner to classic transmembrane RTKs (11). For example, nuclear FGFR3 has been shown in the nucleus of malignant and non-malignant breast epithelial cells (12). A nuclear interaction of FGFR2, STAT5 and progesterone receptor (PR), associated with PR/STAT5-regulated gene expression and breast cancer progression was also reported (13). Other studies have reported nuclear localization and a nucleus-specific function of FGFR1 in non-mammary cells (14-17). Medulloblastoma cells transfected with FGFR1-eGFP and evaluated by immunofluorescence have shown FGFR1 is associated with cell membranes, cytosol and nuclear compartments (17). Substitution of the atypical TMD of FGFR1 (β-sheet containing polar amino acids) with the typical TMD of FGFR4 (α–helical, hydrophobic) prevents the nuclear localization of FGFR1 (18). Inability of both the full-length and cleaved forms of FGFR1 to localize to the nucleus results in reduced migration and invasiveness of cancer cells (15,

16). Finally, ChIP-seq studies revealed that FGFR1 binds nuclear transcription factors involved in neural and muscle development (19).

Amplification of the *FGF3/4/19* ligand genes on chromosome 11q12-14 occurs in ~15% of human breast cancers (20, 21). Notably, one-third of *FGFR1*-amplified tumors also harbor amplification of *CCND1*, *FGF3*, *FGF4* and *FGF19* (22). This co-amplification has been associated with resistance to estrogen deprivation in ER+ breast cancer and poor patient outcome (22), suggesting the possibility of ligand-receptor cooperativity.

Herein, we investigated the mechanisms by which *FGFR1* amplification confers resistance to antiestrogen therapy in ER+ breast cancers. In a cohort of patients treated with the aromatase inhibitor letrozole, we observed that ER+ cancers with concurrent *FGFR1* and *FGF3/4/19* amplification maintained their proliferation despite drug-induced estrogen deprivation and exhibited nuclear localization of FGFR1. We hypothesized that aberrant FGFR1 signalling is causally associated with resistance to estrogen deprivation. Indeed, we show herein that estrogen deprivation leads to an increase of total and nuclear FGFR1 expression as well as FGF3/4/19 ligand expression. We also provide evidence that FGFR1 couples with ERα to drive estrogen-independent transcription of ERα-responsive genes. Finally, we show that dual pharmacological inhibition of FGFR1 and ERα can reduce the growth of patient-derived ER+/*FGFR1*-amplified xenografts. We propose this physical interaction between FGFR1 and ERα provides a mechanistic explanation for how *FGFR1* amplification contributes to endocrine therapy resistance and poor outcome of patients with ER+ breast cancer.

## METHODS

**Clinical trial and tumor biopsies.** Tumor samples were obtained from patients with stage I-III operable ER+/HER2– breast cancer enrolled in a clinical trial of the aromatase inhibitor letrozole administered for 2 weeks prior to surgery (NCT00651976) (23). Patients provided written informed consent according to a protocol approved by the Vanderbilt-Ingram Cancer Center Institutional Review Board. Intra-operative biopsies or surgical specimens, snap-frozen in liquid nitrogen and formalin-fixed paraffin-embedded (FFPE), were obtained from each patient's tumor. Immunohistochemistry (IHC) was conducted in both the pretreatment biopsy and in the post-treatment surgical biopsy of both tumors for Ki67 (Dako #M7240), ER (Santa Cruz #sc542) and PR (Dako #M3569). IHC for ER and PR was conducted according to methods reported elsewhere (24). FFPE tumor sections were scanned at 100x magnification, and the area containing the highest number of positive cells was selected. Positive and negative tumor cells were manually counted at 400x; the percentage of positive cells was calculated with at least 1,000 viable cells. Ki67 IHC was scored by two independent pathologists (MVE and JMG).

**Cell Lines.** Cell lines were obtained from ATCC and maintained in DMEM/10% fetal bovine serum (FBS; Gibco). Long-term estrogen-deprived (LTED) cells were generated upon long-term culture in phenol red-free IMEM/10% dextran-charcoal-treated FBS [DCC-FBS; Hyclone, contains <0.0367 pM 17β-estradiol (E2)] for 3-8 months until exponentially-growing, hormone-independent cells emerged as described previously (25). Cell lines were authenticated by ATCC prior to purchase by the STR method. Cell lines were not authenticated after purchase. Mycoplasma testing was conducted for each cell line before use. All experiments were performed less than 2 months after thawing early passage cells.

***FGFR1* and *CCND1* fluorescence *in situ* hybridization (FISH) analysis.** Four-μm tissue sections were mounted on charged slides and hybridized overnight with the SPEC *FGFR1/CEN8* Dual Color Probe (ZytoVision, catalog# Z-2072-200) and *CCND1/CEN11* Dual Color Probe (ZytoVision, catalog# Z-2071-200). Briefly, deparaffinization, protease treatment and washes were performed as

per standard protocols. After this pretreatment, the slides were denatured in the presence of 10 μL of the probe for 6 min at 72°C, and hybridized at 37°C overnight in StatSpin (Thermobrite, Abbott Molecular, Inc.). Post-hybridization saline-sodium citrate washes were performed at 72°C and the slides were then stained with DAPI before analysis. Normal vessels, fibroblasts and/or non-tumor tissues served as internal positive controls. Cases were further evaluated only if diploid nuclei in normal tissues displayed one or two clearly distinct signals of each color. Tumor tissue was scanned for amplification hot spots under 40× magnification (Olympus BX60 Fluosescent microscope). If the *FGFR1* or *CCND1* signals were homogeneously distributed, then random areas were used for counting the signals. Twenty to sixty tumor cell nuclei from random areas were individually evaluated with the 100× oil immersion objective by counting green *FGFR1* and orange centromere 8 (for FGFR1), or orange *CCND1* and green centromere 11 (for CCND1) signals. The *FGFR1/CEN8* or *CCND1/CEN11* ratio and the average *FGFR1* or *CCND1* copy number per cell were calculated next. Cases were considered to be *FGFR1* or *CCND1* amplified under one of the following conditions:

a) *FGFR1/CEN8* or *CCND1/CEN11* ratio ≥2.0;

b) average number of *FGFR1* or *CCND1* signals per tumor cell nucleus ≥6

**Cell proliferation.** Cells were plated in 10% DCC-FBS ± FGF3 100 ng/mL or ± 2 μM lucitanib for 7 or 14 days before being trypsinized and counted using a Coulter Counter (Beckman Coulter), or fixed and stained with crystal violet followed by quantification by spectrophotometric detection at 490 nm using a plate reader (GloMax®-Multi Detection System, Promega). *Clonogenic assays*. Cells ($5x10^4$ /well) were seeded in triplicate in medium with 10% DCC-FBS in 6-well plates and then treated with ± 100 ng/mL FGF3 ± 2 μM lucitanib or 1 μM ICNB054828. Media, FGF ligands, and drugs were replenished every 3 days until 50-70% confluency was observed in control wells. Monolayers were then fixed and stained with 20% methanol/80% water/0.5% crystal violet for 20 min, washed with water, and dried. After photographic images of the plates were obtained, the crystal violet stain was solubilized with 20% acid acetic and the image intensity of the monolayers was

quantified by spectrophotometric detection at 490 nm using a plate reader (GloMax®-Multi Detection System, Promega). *siRNA transfection experiments.* Cells were reverse transfected into 100-mm dishes using Lipofectamine RNAiMAX® (Invitrogen) and 25 nM siRNA [siControl-Ambion cat. #4390843; si*FGFR1*- Ambion cat. #AM16708; si*FGFR1*- Ambion cat. #AM51331]. The next day, $5x10^4$ cells/well were reseeded in IMEM/10% DCC-FBS in 6-well plates for proliferation assays or in 60-mm plates for immunoblot analysis. For proliferation assays, media was changed 72 h after transfection to IMEM/10% DCC-FBS + 100 ng/mL FGF3 and every 3 days thereafter. Cells were trypsinized 7 days post-transfection and counted using a Coulter Counter (Beckman Coulter). For immunoblot analyses, cells were harvested and protein lysates prepared on day 3 post-transfection. *Three-dimensional Matrigel culture*. Cells (~$1x10^4$ /well) were seeded in 48-well plates in triplicate. Before seeding, cells were suspended in their respective medium on growth factor–reduced Matrigel (BD Biosciences) as described previously (26). Ligands and/or inhibitors were added at the time of cell seeding and replenished with fresh medium every 3 days. After 6 or 12 days, images were captured from at least 3 different fields using a CK 40 microscope. Cell viability was measured by MTT assay and the number of colonies per well was quantified by Gelcount® scanning.

**Proximity ligation assay (PLA).** *FGFR1 expression and localization.* PLA was performed using FGFR1 (Abcam, cat. #10646, rabbit) antibody. Cells ($5x10^4$ /well) were seeded in 16-well chamber slides (Lab-Tek) in triplicate in their respective growth medium and then serum-starved for 24 h. PLA was performed as per the Duolink *in situ* PLA™ protocol (Olink Bioscience, Sweden). To visualize the bound antibody pairs, the Duolink Detection Kit (#DUO92101 –Sigma) with PLA plus and minus probes for rabbit (anti-rabbit plus #DUO92002, anti-rabbit minus #DUO92005 -Sigma for FGFR1) were used according to the manufacturer's protocol. Slides were mounted with the Duolink Mounting Medium and stained with DAPI (82040-0005). Analysis was performed by confocal microscopy (LSM710, ZEISS) and the number of red dots (FGFR1) was quantitated by Duolink Image Tool software; 8-15 random fields per sample were analyzed.

*FGFR1-ERα association and localization.* PLA was performed using FGFR1 (Abcam, cat. #10646, rabbit) and ERα (Santa-Cruz, cat. #8002, mouse) antibodies. Cells ($5x10^4$ /well) were seeded in 16-well chamber slides (Lab-Tek) in triplicate in their respective growth medium and serum starved for 24 h. PLA (Duolink in situ PLA$^{TM}$; Olink Bioscience, Sweden) was performed to detect FGFR1/ERα complexes. To visualize the bound antibody pairs, the Duolink Detection Kit (#DUO92101, Sigma) with PLA plus and minus probes for rabbit (anti-rabbit plus, #DUO92002, Sigma) and PLA plus and minus probes for mouse (anti-mouse minus, #DUO92004, Sigma) were used according to the manufacturer's protocol. Slides were mounted with the Duolink Mounting Medium and stained with DAPI (Sigma 82040-0005). Analysis was performed by confocal microscopy (LSM710, ZEISS) and the number of red dots (indicating FGFR1/ERα complexes) was quantitated by the Duolink Image Tool software; 8-15 random fields per sample were analyzed. In addition to cells on slides, PLA was performed in 5-μm thick sections from paired pre- and post-letrozole FFPE tumor blocks from patients in the clinical trial. Tumor sections were de-paraffinized and subjected to antigen retrieval by microwave cooking in 0.01M citrate buffer (pH 6.0) at 1000 W for 30 min. After incubation in blocking buffer (1X PBS + 10% BSA + 0.3 % Triton X-100), the slides were incubated overnight with FGFR1 (Abcam, cat. #10646, rabbit) and ERα (Santa-Cruz, cat. #8002, mouse) antibodies. PLA (Duolink in situ PLATM; Olink Bioscience, Sweden) was performed to detect FGFR1/ERα complexes and their localization. To visualize the bound antibody pairs, the Duolink Detection Kit (#DUO92101, Sigma) with PLA plus and minus probes for rabbit (anti-rabbit plus, #DUO92002, Sigma) and PLA plus and minus probes for mouse (anti-mouse minus, #DUO92004, Sigma) was used according to the manufacturer's protocol. Slides were mounted with the Duolink Mounting Medium and stained with DAPI (Sigma 82040-0005). Analysis was performed by confocal microscopy (LSM710, ZEISS) and the number of red dots (FGFR1/ERα complexes) was quantified by Duolink Image Tool software; 8-15 random fields per sample were analyzed.

**Viral transduction.** FGFR1 wild-type and GFP-expressing lentiviral constructs were generated in the pLX302 Gateway vector (Open Biosystems); FGFR1/TK- (K514M) pLX302 was created by site-

directed mutagenesis by Genewiz (New Jersey, USA). To generate stably-transduced lines, 4 μg of the FGFR1, FGFR1/TK– (K514M), and GFP-pLX302 constructs were co-transfected with 3 μg psPAX2 (plasmid encoding gag, pol, rev, and Tat genes), and 1 μg pMD2G envelope plasmid (Sigma Aldrich) into 293FT cells using Lipofectamine 2000 (Thermo Fisher). 293FT growth media was changed 24 h post-transfection; virus-containing supernatants were harvested 48 and 72 h post-transfection, passed through a 0.45-μm filter, diluted 1:4, and applied to target cells with 8 μg/mL polybrene (Sigma Aldrich). Virus-producing cells were selected in 1 μg/mL puromycin. Empty pMXs-puro and pMXs-puro retroviral constructs expressing FGFR1 wild-type and FGFR1/TMD FGFR4 were generated by PCR-based cloning by Genewiz. To generate stably-transduced cells, 1 μg of the pMXs-puro retrovirus was co-transfected with 1 μg pCMV-VSVG (vesicular stomatitis virus surface protein envelope plasmid) into HEKgpIRES cells (HEK293 cells stably harboring a gag-pol internal ribosome entry site) using Lipofectamine 2000. Virus harvest and target cell infection were performed as above for the lentiviral constructs.

**Gene Expression Analyses.** CAMA1 cells were plated in estrogen-free media and treated ± 100 ng/mL FGF3/19 (Sigma) for 6 h. Cells were harvested and RNA was purified using the RNeAsy kit (Qiagen, Valencia, CA); cDNA was generated using High Capacity cDNA Reverse Transcription Kits (Applied Biosystems, Carlsbad, CA) followed by analysis of ERα pathway genes using the Estrogen Receptor PCR Array (Qiagen, PAHS-005Z). RNA sequencing data (see "RNA Sequencing and cDNA library construction" below) were aligned to human genome version 19 using the splice-aware aligner TopHat (v2.0.9), and isoform level expression was quantified using cufflinks. Expression levels were normalized across the data set using cuffnorm. We compared genes upregulated in *FGFR1*-amplified vs *FGFR1* non-amplified cancers [≥2.0 fold, false discovery rate (FDR)-adjusted $p \leq 0.05$]. These genes were entered into Gene Set Enrichment Analysis (GSEA) as a ranked list. Gene sets with an FDR of <0.01 were considered enriched between *FGFR1*-amplified vs. non-amplified tumors.

**Chromatin immunoprecipitation/next generation DNA sequencing (ChIP).** ChIP was done using CAMA1 cells plated in estrogen free media ± 100 ng/mL FGF3 and treated with 2 μM lucitanib, 1 μM fulvestrant or the combination. Cells were grown to 80% confluency, washed 3x in ice-cold PBS, and then fixed for 10 min at room temperature using 7% formaldehyde. The formaldehyde was quenched with 2.5 M glycine; cells were lysed using Farnham lysis buffer first and then with nuclei lysis buffer (50 mM Tris-HCl pH 8.0, 10 mM EDTA pH 8.0, 1% SDS). The chromatin was sonicated using a Covaris LE220 with the following conditions: 35 min at peak power 350, duty factor 15, 200 cycles/burst, and average power 52.5; 200 μL of the chromatin was saved for input. Sonicated chromatin was diluted using ChIP Dilution Buffer (50 mM Tris-HCl pH 8.0, 0.167 M NaCl, 1.1% Triton X-100, 0.11% sodium deoxycholate), RIPA-150, protease inhibitors, and sodium butyrate. ERα (sc-8002) and FGFR1 (ab10646) antibodies were linked to magnetic anti-mouse and anti-rabbit Dynabeads respectively, and then incubated with chromatin for >12 h at 4°C. Immunoprecipitates (IPs) were washed with the following buffers (RIPA-150, RIPA-500, RIPA-LiCl, and TE Buffer) for 5 min each. Chromatin-IPs were eluted from the beads, treated with RNAse A at 65°C with shaking for 4 h to reverse crosslinks, followed by Proteinase-K treatment at 55°C for 1 h. Next, DNA was purified using phenol-chloroform extraction followed by ethanol precipitation and subsequent quantification by Qubit. Standard Illumina ChIPseq library kits were used to build sequencing libraries. The resulting libraries were sequenced at Vanderbilt Technologies for Advanced Genomics (VANTAGE) Core Resource as SR50 on a HiSeq3000. Each IP was sequenced with a matching input. The resulting sequencing files were aligned to human genome version 19 by BWA (Burrows-Wheeler Aligner). For each replicate, peaks were called comparing to matched input, using MACS14 and default settings. The intersection of peak calls from each replicate was used to define the peak call set for each condition. Peaks were assigned to closest genes using annotatePeaks.pl in the HOMER analysis suite and heatmaps were generated using ngs.plot.

**Chromatin immunoprecipitation/quantitative PCR (ChIP-qPCR).** ChIP was performed in CAMA1 cells as described above. DNA was analyzed by real-time qPCR in triplicate with Sso

Advanced SYBR Green Supermix (Bio-Rad) in a CFX qPCR machine (Bio-Rad). The fold-enrichment of ChIP samples was calculated using the $2^{\Delta Ct}$ (threshold cycle) method. Ct values for ERα-ChIP and FGFR1-ChIP samples were normalized to input DNA Ct values, and then independently to respective Negative Control Ct values to account for antibody background. Primer sequences are listed in Table S1.

**RNA Sequencing and cDNA library construction.** Core biopsies were flash frozen in liquid $N_2$ and stored at -80°C until RNA extraction was performed as described elsewhere (27). Total RNA was quantified using the Quant-iT™ RiboGreen® RNA Assay Kit (Invitrogen) and normalized to 4 ng/μL; 200 ng of each sample were used for library preparation in an automated variant of the Illumina Tru Seq™ RNA Sample Preparation protocol (Revision A, 2010). This method uses oligo(dT) beads to select mRNA from the total RNA sample and is followed by heat fragmentation and cDNA synthesis from the RNA template. The resultant cDNA then goes through library preparation (end repair, base 'A' addition, adapter ligation, and enrichment) using Broad Institute-designed indexed adapters for multiplexing. After enrichment, libraries were quantitated with qPCR using the KAPA Library Quantification Kit for Illumina Sequencing Platforms and pooled equimolarly. The entire process is performed in a 96-well format with all pipetting done by either the Agilent Bravo or PerkinElmer JANUS Mini liquid handlers.

**Non-stranded Illumina RNA-sequencing.** Pooled libraries were normalized to 2 nM and denatured using 0.2 N NaOH prior to sequencing. Flowcell cluster amplification and sequencing were performed according to the manufacturer's protocol using either the HiSeq 2000 v3 or HiSeq 2500. Each run was a 76-bp, paired-end run with an eight-base index barcode. Data were analyzed using the Broad Picard Pipeline, which includes de-multiplexing and data aggregation. TopHat spliced aligner software was used to map sequencing reads and to generate a BAM file for each tumor (28). RNAseq GCT files were generated from BAM files using RNA-SeQC (29).

**Xenograft studies.** We used two ER+/HER2-/*FGFR1*-amplified patient-derived xenografts (PDXs). PDX T272 (XenTech) required estrogen supplementation in the drinking water (8.5 mg/L estrogen)

to grow as tumors in female athymic nude mice (Envigo). The second PDX, TM00368 (Jackson Laboratory), was implanted in female ovariectomized SCID/beige mice (Jackson Laboratory) implanted with a s.c. 21-day relase, 0.25-mg 17β-estradiol pellet (Innovative Research of America). Tumors were serially transplanted in athymic or SCID/beige mice under general anesthesia. When xenografts reached an average size of ≥200 $mm^3$, mice were randomized to treatment with vehicle, lucitanib (10 mg/kg/day p.o. for T272 or 7 mg/kg/day p.o. for TM00368), fulvestrant (5 mg/week s.c.) or both drugs (n= 10 per group for T272 and n= 8 per group for TM00368). Tumors diameters were measured using calipers twice a week, and volume in $mm^3$ was calculated with the formula: volume = $width^2$ x length/2. When tumor volume exceeded 2 $cm^3$ or at end of treatment, mice were sacrificed and tumors harvested 1 h after the last dose of lucitanib. Portions of tumors were snap frozen or fixed in 10% neutral buffered formalin and embedded in paraffin for subsequent analyses. Five-μm paraffinized sections were used for IHC using Y653/54 phosphorylated FGFR1 (Abcam #111124) and ERα (Santa Cruz Biotech #8002). Sections were scored by an expert pathologist (M.V.E.) blinded to the treatment.

**Immunoprecipitation and immunoblot analyses.** Cells were lysed in RIPA buffer (for immunoblot) or in NP-40 buffer containing protease and phosphatase inhibitors (for immunoprecipitation), and sonicated for 10 sec; debris was separated by centrifugation at 18,000 x*g* for 10 min at 4°C. Protein concentration in the supernatants was measured using the BCA assay (Pierce). FGFR1 was precipitated from cell lysates with a FGFR1 C-terminal antibody (Abcam #76464) or a FGFR1 N-terminal antibody (Cell Signaling #3472) for 16 h at 4°C. Whole cell lysates and immune complexes were separated by SDS-PAGE, transferred to nitrocellulose, and subjected to immunoblot analyses as described previously (30) using primary antibodies against ERα, FRS2α (Santa Cruz Biotech.), AIF, tubulin, lamin A/C, actin, phosphorylated FRS2α (T436) (Cell Signaling) and FGFR1 (Abcam). HRP-conjugated anti-rabbit and anti-mouse were used as secondary antibodies (Santa Cruz Biotechnology). Immunoreactive proteins were visualized by enhanced chemiluminescence (Pierce, Rockford, IL, USA). Membranes were cut horizontally to probe with

multiple antibodies. Blots probed with phospho-antibodies were stripped with Restore Western Blot Stripping Buffer (Thermo Fisher Scientific) and re-probed with antibodies to the total protein.

**Membrane, cytoplasmic, nuclear soluble and chromatin-bound fractionation.** CAMA1 and CAMA1$^{FGFR1}$ cells were subjected to fractionation using a cell fractionation kit (Thermo Scientific #78840) according to the manufacturer's protocol. Adequacy of fractionation was confirmed by immunoblot of cell fractions with antibodies against apoptosis-inducing factor (AIF; plasma membrane), tubulin (cytoplasm), lamin A/C (nucleus) and histone H1 (chromatin bound).

**Inhibition of nuclear export**. CAMA1 and CAMA1$^{FGFR1}$ ($1x10^5$) cells were grown in chamber slides and treated with vehicle or 30 ng/mL leptomycin B for 2 h and then fixed with PBS containing 3.7% formaldehyde, washed with PBS, permeabilized with PBS containing 0.25% Triton-X-100, blocked with PBS containing 10% BSA and 0.1% Tween-20, and incubated overnight with a FGFR1 (Abcam, cat. #10646, rabbit) primary antibody diluted in blocking solution. Slides were washed and incubated with goat-derived Alexa Fluor® 594-conjugated antibodies and mounted with ProLong® Gold Antifade mounting media (Life Technologies). IF analysis was performed by confocal microscopy (LSM710, ZEISS); nuclear cell fluorescence was quantified by ImageJ using 8-15 random fields per sample.

**Statistics**. Results are representative of 3 independent experiments. Results are expressed as the mean, and error bars indicate SEM. A P value of less than 0.05 was considered statistically significant.

**Study approval.** Animal studies were approved and performed in accordance with the Vanderbilt Institutional Animal Care and Use Committee.

## RESULTS

***FGFR1* amplification and overexpression is associated with endocrine resistance in ER+ breast cancer.** We studied 72 tumor biopsies from post-menopausal women with clinical stage I-III operable, ER+/HER2– breast cancer treated with the aromatase inhibitor letrozole for 2 weeks prior to surgery (NCT00651976). Earlier studies have demonstrated that a Ki67 score 2 weeks after antiestrogen therapy can be utilized to predict which tumors are endocrine sensitive or resistant, as well as their odds of recurrence following adjuvant endocrine therapy (31). We applied these metrics to our tumor set and categorized 40 tumors as sensitive [natural log (ln) of post-letrozole Ki67 ≤1.0 or ≤2.4% tumor cells], 11 tumors as intermediate responders (ln=1.1-1.9 or 2.5-7.3% tumor cells), and 21 tumors as resistant (ln ≥2.0 or ≥7.4% tumor cells; Fig. 1A). *FGFR1* copy number was determined in tumor sections by fluorescence *in situ* hybridization (FISH). We observed *FGFR1* amplification in 9/21 (43%) resistant tumors compared to 3/40 (7%) sensitive tumors and 1/11 (10%) intermediate tumors (resistant vs. intermediate and sensitive tumors; $p$=0.0011; Fig. 1B). To correlate *FGFR1* copy number with protein levels, we performed immunohistochemistry (IHC) in tumors from the trial. FGFR1 protein levels correlated with gene amplification by FISH. In *FGFR1*-amplified cancers, we observed a significant increase in total and nuclear FGFR1 in post-treatment compared to pre-treatment biopsies ($p$<0.05; Fig. 1C,E). A letrozole-induced increase in both total and nuclear FGFR1 was not observed in tumors without *FGFR1* amplification (Suppl. Fig. 1A).

**Estrogen deprivation increases nuclear and cytosolic FGFR1 expression.** To examine whether this same modulation of FGFR1 levels occurred in more controlled experimental models, we tested five ER+/HER2– human breast cancer cell lines with and without *FGFR1* gene amplification as determined by FISH: CAMA1, MDA-MB-134 and HCC1500 cells are *FGFR1* amplified while MCF-7 and ZR75.1 cells are not (Suppl. Fig. 2A). *FGFR1* amplification correlated with FGFR1 protein levels; MDA-MB-134 and HCC1500 cells express both full-length and cleaved FGFR1 while only full-length FGFR1 was detected in CAMA1 cells (Suppl. Fig. 2B). To mirror the acute estrogen deprivation induced by letrozole in primary tumors in the clinical trial (32), we cultured the *FGFR1*-

amplified cell lines in estrogen-free medium for 4-6 days. This resulted in an increase in FGFR1 expression in all *FGFR1*-amplified lines (Fig. 2A). Specifically, we observed an increase in full-length FGFR1 in CAMA1 cells, of both cleaved and full-length FGFR1 in MDA-MB-134, and only the cleaved form in HCC1500 upon estrogen withdrawal.

To determine whether long-term estradiol deprivation also affected FGFR1 expression, we generated three long-term estrogen-deprived (LTED) cell lines as previously described (25): CAMA1$^{LTED}$ and MDA-MB-134$^{LTED}$ (*FGFR1*-amplified) and MCF-7$^{LTED}$ (*FGFR1* non-amplified). As we had observed with acute estrogen-deprivation, CAMA1$^{LTED}$ and MDA-MB-134$^{LTED}$ cells exhibited increased expression of full-length and cleaved FGFR1, respectively, whereas MCF-7$^{LTED}$ cells showed a reduction in FGFR1 expression compared to parental MCF-7 cells. The LTED lines displayed an increase in ERα levels compared to their parental counterparts (Fig. 2B). Immunofluorescence (IF) by confocal microscopy confirmed the increase in total and nuclear FGFR1 in CAMA1$^{LTED}$ vs. parental cells (Fig. 2C).

To confirm that FGFR1 localizes to the nucleus we substituted the atypical TMD of FGFR1 (β-sheet containing polar amino acids) with the typical α–helical, hydrophobic TMD of FGFR4, previously shown to prevent nuclear localization of FGFR1 (18). CAMA1 cells transfected with FGFR1 harboring the TMD of FGFR4 (referred to as CAMA1$^{FGFR1/TMD\text{-}FGFR4}$) showed a reduction in both nuclear soluble and chromatin-bound FGFR1 relative to CAMA1 cells transfected with wild-type FGFR1 (Fig. 2D,E). Similar to FGFR1-transfected CAMA1 cells, parental CAMA1 cells also exhibited nuclear soluble and chromatin-bound FGFR1 at steady state (Suppl. Fig. 2C). Further, treatment with nuclear export inhibitor leptomycin B (33), resulted in an increase in nuclear FGFR1 as measured by IF in both parental (Fig. 2F) and FGFR1-transfected CAMA1 cells (Suppl. Fig. 2D). Knockdown of *FGFR1* with siRNA confirmed the specificity of the FGFR1 antibody used for both immunoblot and IF analyses (Suppl. Fig. 2E,F).

**FGF3/4/19 expression is upregulated upon estrogen deprivation.** Approximately 30-40% of *FGFR1*-amplified breast cancers exhibit amplification of *CCND1, FGF3, FGF4* and *FGF19* in

chromosome 11q12-14 (34). Co-amplification of these genes has been shown to be associated with reduced patient survival (22). By interrogating The Cancer Genome Atlas (TCGA), we found that among the 13% of breast cancers with *FGFR1* amplification, 36% of these tumors also harbor *11q-12-14* amplification (Suppl. Fig. 3A,B) (35, 36). Outcomes analysis of Kaplan Meier-plotter [breast cancer] showed that patients with co-amplification of *FGFR1* and *CCND1/FGF3/FGF4/FGF19* treated with antiestrogen therapy exhibit a shorter time to relapse compared to patients without co-amplified tumors (hazard ratio=1.75; Suppl. Fig. 3C) (37). Based on this analysis, we investigated the presence of *FGFR1* and *11q12-14* co-amplification in our cohort of patients treated with letrozole. In this study, 8 of 9 (90%) *FGFR1*-amplified tumors exhibited co-amplification of *FGF3/4/19* and this co-amplification strongly correlated with resistance to estrogen deprivation with letrozole ($p$=0.0001; Fig. 3A). These data suggest that co-amplification of *11q12-14* and *FGFR1* plays a potentially causal role in resistance to endocrine therapy in hormone-dependent breast cancers.

We then analyzed *11q12-14* amplification by FISH in ER+ breast cancer cells. All *FGFR1*-amplified cell lines exhibited co-amplification of *11q12-14* (Fig. 3B, Suppl. Fig. 4A); *FGFR1* non-amplified MCF-7 cells did not. Supporting a correlation of copy number with gene expression, all *11q12-14*-amplified cell lines expressed markedly higher *FGF3/4/19* mRNA levels by qRT-PCR compared to MCF-7 cells (Fig. 3C). Similar to the effect on FGFR1 protein levels, 24 h of estrogen deprivation increased *FGF3/4/19* mRNA expression 1.5- to 2-fold in all *FGFR1*-amplified cell lines (Suppl. Fig. 4B). This increase was even more substantial when we investigated the transcript expression of *FGF3/4/19* in LTED *FGFR1*-amplified cells. In contrast, MCF7$^{LTED}$ cells exhibited little or no increase in FGF ligands mRNA compared to MCF-7 parental cells (Fig. 3D).

These results also suggested that an excess of FGFs could accelerate the growth of ER+/*FGFR1*-amplified cells in estrogen-free conditions. To test this, we stimulated estrogen-starved CAMA1 cells ± FGF3. Exogenous FGF3 enhanced cell growth compared to unstimulated cells. Both treatment with the FGFR1 tyrosine kinase inhibitor (TKI), lucitanib (38) (Fig. 3E), and transfection with an FGFR1 siRNA prevented this outgrowth (Fig. 3F).

**Long-term estradiol deprivation increases the interaction of FGFR1 with ERα.** The association of FGFR1 with other nuclear proteins, such as ribosomal S6 kinase (RSK1) and CREB-binding protein (CBP), is required for the ability of nuclear FGFR1 to induce target gene expression in medulloblastoma and neuroblastoma cells (39). The interaction between FGFR1 and ERα has been reported to mediate lactotroph proliferation in the pituitary gland (40). Thus, we investigated this interaction in ER+/FGFR1 amplified breast cancer cells. Immunoprecipitation of FGFR1 from MDA-MB-134, CAMA1 and CAMA1$^{LTED}$ whole cell lysates co-precipitated ERα in all three cell lines (Fig. 4A). This association was stronger in MDA-134 and CAMA1$^{LTED}$ cells compared to parental CAMA1 cells. We next confirmed the FGFR1-ERα association in CAMA1 and CAMA1$^{LTED}$ nuclear extracts after precipitation with both C-terminal and N-terminal FGFR1 antibodies (Fig. 4B), consistent with presence of full-length FGFR1 in cell nucleus. To quantitate this interaction, we performed proximity ligation assays (PLA). An interaction between FGFR1 and ERα was observed in the cytoplasm and nucleus of CAMA1 and CAMA1$^{LTED}$ cells by PLA, particularly in in the latter (Fig. 4C,D), in line with the immunoprecipitation experiments. Treatment with either lucitanib or fulvestrant reduced FGFR1/ERα complexes (Fig. 4E,F), suggesting this interaction requires FGFR1 tyrosine kinase (TK) activity.

To explore further whether the TK function of FGFR1 is required for FGFR1-ERα complex formation, CAMA1 cells were transduced with constructs expressing GFP, wild-type FGFR1 or a TK dead K514M FGFR1 mutant (FGFR1/TK–). Overexpression of wild-type FGFR1 increased detectable FGFR1-ERα complexes while overexpression of FGFR1/TK– decreased them as measured by PLA (Fig. 4G,H). Steady-state levels of pFRS2 were upregulated in cells transduced with wild-type FGFR1 but not with the FGFR1/TK– mutant (Suppl. Fig. 5A). Importantly, the CAMA1$^{FGFR1/TK–}$ cells were not able to grow in the absence of estradiol (Suppl. Fig. 5B,C). These data suggest that FGFR1 TK activity is important for the association of FGFR with ERα. Finally, we observed an increase of FGFR1-ERα complexes in post-letrozole compared to paired pre-letrozole

FFPE tumor sections from two breast cancer patients harboring tumor co-amplification of *FGFR1* and *11q12-14* (Fig. 4I,J).

**FGFs/FGFR pathway modulates ERα-DNA binding.** To evaluate estrogen-independent genomic functions of ERα in ER+/*FGFR1* amplified cells, we performed chromatin immunoprecipitation followed by next-generation sequencing (ChIP-seq) in estrogen-deprived CAMA1 cells ± FGF3. Treatment with FGF3 shifted both ERα and FGFR1 to new binding sites that were unoccupied in the absence of the FGF ligand. (Suppl. Fig. 6A,B). We identified 1120 and 553 regions (peaks) by ERα-ChIP and FGFR1-ChIP, respectively, that were significantly enriched upon FGF3 treatment. Treatment of CAMA1 cells with each fulvestrant or lucitanib alone or in combination reduced ERα or FGFR1 DNA binding to these new sites (Fig. 5A,B). These results were validated by ChIP-PCR (Suppl. Fig. 6C,D). As shown in Figure 5C,D, ERα and FGFR1 bound to different ERα-related genes, but treatment with lucitanib, fulvestrant or the combination reduced or abrogated this binding.

To identify the functional output of estrogen-independent ERα activity, we classified the genes identified by FGFR1 and ERα ChIP-seq using gene set enrichment analysis (GSEA). The top enriched gene sets included *epithelial mesenchymal transition*, *STAT5 signaling*, *estrogen response early genes* and *p53-pathways* (all *FDR* <0.009) after FGFR1 ChIP-seq (Fig. 5E); and *estrogen response early genes*, *estrogen response late genes*, *K-Ras signaling* and *p53-pathways* (all *FDR* <0.0001) after ERα ChIP-seq (Fig. 5F). To apply these findings to primary ER+ breast cancers, we performed RNA sequencing analysis on 7 *FGFR1*-amplified and 25 *FGFR1* non-amplified tumors treated in the clinical trial with letrozole. The Volcano-plot in Fig. 5G shows that, of >24,000 genes analyzed, 280 gene transcripts were increased >2 fold in *FGFR1*-amplified compared to *FGFR1* non-amplified cancers ($p$<0.01; red dots in Fig. 5G). The top enriched genes by GSEA in *FGFR1* amplified patients included *G2M checkpoint* genes, *E2F target* genes, *estrogen response late genes* and *estrogen response early genes* (all *FDR* <0.01; Fig. 5H and Suppl. Fig. 7). These results further suggest that the ERα pathway is still active in estrogen-deprived (upon letrozole treatment) ER+/*FGFR1*-amplified primary tumors.

**FGFR1 signaling induces expression of ERα-dependent genes.** Based on the ChIP-seq results and to elucidate further the role of the FGF/FGFR1 axis on ERα signaling, we performed a qRT-PCR profiling assay including 84 ERα regulated genes. FGF3/19 stimulation of estrogen-deprived CAMA1 cells induced >2-fold mRNA expression of a subset of ERα target genes, including *TFF1*, *CCND1*, *THSB1*, *CTGF*, *CCL2* and *EGR3* (Fig. 6A). Both FGF3 and FGF19 induced *EGR3*, *CCND1* and *THSB1* mRNA; this induction was inhibited by treatment with lucitanib, fulvestrant or the combination (Fig. 6B,C), and also by transfection of a TK dead K514M FGFR1 mutant into CAMA1 cells (Suppl. Fig. 5D). In line with their higher levels of ERα, FGFR1 and FGF3/4/19 (Figs. 2C, 3D), CAMA1$^{LTED}$ cells expressed higher levels of ERα-regulate genes than CAMA1 parental cells (Suppl. Fig. 8).

To support our results with lucitanib were not due to off-target effects of the small molecule, we tested the FGFR inhibitor INCB054828 (41). Treatment with INCB054828 also blocked FGF3-induced pFRS2, CAMA1 cell growth and ERα target gene expression (Suppl. Fig. 9A-C).

**Combined blockade of FGFR1 and ERα potently inhibits growth of ER+/*FGFR1*-amplified breast cancers.** Treatment with fulvestrant and lucitanib reduced the expression of ERα dependent genes in ER+/*FGFR1*-amplified breast cancer cells (Fig. 6). Thus, we next examined whether FGFR1 and/or ERα inhibitors would have an effect on tumor cell growth. Treatment with the combination of lucitanib and fulvestrant suppressed CAMA1 colony formation in 3D-matrigel significantly more potently than each drug alone (Fig. 7A,B). Western blot analysis of lysates from cells treated for 6 h showed that the only the combination simultaneously reduced levels of pFRS2, pERK1/2 and ERα (Fig. 7C). We next examined the effect of these drugs against two ER+/HER2–/*FGFR1*-amplified patient-derived xenografts (PDXs), T272 and TM00368 (Fig. 7D). Ovariectomized mice with established xenografts (≥250 mm$^3$) were treated with vehicle, lucitanib, fulvestrant or both drugs. PDX T272 but not PDXTM00368 required brief estrogen supplementation to generate tumors. In mice bearing PDX T272, the dose of lucitanib was reduced from 10 to 7 mg/kg/day after 3 weeks of

therapy due to toxicity in both lucitanib-containing arms. Mice with TM00368 PDXs were treated with 7 mg/kg/day lucitanib. Treatment with the combination of fulvestrant and lucitanib inhibited growth of both PDXs more potently than either drug alone (Fig. 7E and Suppl. Fig. 10A). All mice bearing TM00368 xenografts exhibited a ≥50% reduction in tumor size from baseline after 3 weeks of treatment with fulvestrant/lucitanib (Fig. 7F). Biomarkers of response were assessed by IHC in TM00368 tumors harvested at the completion of therapy. Treatment with the combination of lucitanib plus fulvestrant markedly reduced detectable levels of Y653/4 phosphorylated FGFR1 and total ERα (Fig. 7G,H). FGFR1 antibody pulldowns of tumor lysates from vehicle- and lucitanib-treated mice co-precipitated ERα. This was not observed in tumors treated with fulvestrant or the combination (Fig. 7I). No change in mouse weight was observed in any of the treatment arms (Suppl. Fig. 10B,C).

## DISCUSSION

We report herein a novel mechanism by which *FGFR1* amplification confers resistance to antiestrogen therapy in ER+ breast cancers. In a cohort of post-menopausal patients treated with the aromatase inhibitor letrozole, cancers with *FGFR1* and *FGF3/4/19* amplification retained tumor cell proliferation, suggesting aberrant FGFR1 signaling is associated with resistance to estrogen deprivation. Short and long-term estrogen deprivation increased total and nuclear FGFR1 and FGF ligand expression in ER+/*FGFR1*-amplified breast cancer cells and primary tumors. This was associated with an increase in nuclear FGFR1/ERα complexes and maintenance of estrogen-independent transcription of ER-responsive genes. The interaction between FGFR1 and ERα was blocked by a kinase-dead FGFR1 mutant or by FGFR tyrosine kinase inhibitors. ChIP-seq analysis of FGF-stimulated *FGFR1*-amplified cells showed binding of FGFR1 and of ERα to DNA, which was inhibited by the FGFR TKI lucitanib and by the ER downregulator fulvestrant, respectively, suggesting a possible inter-dependence between FGFR1 and ERα at transcription start sites. Of note, RNA-seq data from ER+/*FGFR1*-amplified tumors from patients treated with letrozole suggested the ERα pathway is still active (Fig.5G,H), thus providing a plausible explanation for maintenance of proliferation in these estrogen-deprived cancers. Finally, dual pharmacological inhibition of FGFR1 and ERα potently inhibited growth of ER+/*FGFR1*-amplified breast cancer cells and PDX models, supporting the clinical development of this combination in patients with this subtype of breast cancer.

The association of FGFR1 with other nuclear proteins is required for the ability of nuclear FGFR1 to induce target gene expression in other cancers (39). Since FGFR1 inhibition reduced the transcription of ERα related genes, we speculated the previously reported transcriptional function of FGFR1 (16, 19, 39, 42) may play a role in resistance to estrogen deprivation. Of note, we precipitated both FGFR1 and ERα with C-terminal and N-terminal FGFR1 antibodies from *FGFR1*-amplified CAMA1 cell nuclei (Fig. 4B), suggesting that full-length FGFR1 associates with ERα in the nucleus. These findings were supported by PLA and confocal microscopy studies (Fig. 4C). Inhibition of

FGFR1 TK activity with lucitanib and expression of a TK dead K514M FGFR1 mutant into CAMA1 cells reduced ERα-dependent gene transcription (Fig. 6B-C and Suppl. Fig. 5D) and inhibited the association of FGFR1 with ERα (Fig. 5E-H). Taken together, these data support a novel TK-dependent role of nuclear FGFR1 on ERα-dependent gene transcription in estrogen-independent ER+/*FGFR1*-amplified breast cancers.

To the best of our knowledge, this is the first report of a physical association of FGFR1 and ERα associated with antiestrogen resistance. It follows studies supporting both the nuclear localization and nuclear function of FGFR1. FGFR1 can enter the nucleus by retrograde transport from the endoplasmic reticulum lumen to the cytosol via Sec61p channels before endoplasmic vesicles deliver the receptor to the plasma membrane (17, 43). This process is possible because of the atypical TMD of FGFR1, which consists of non-polar amino acid chains interrupted by polar regions in a β-sheet structure, thus allowing mobilization of the receptor out of the membrane (17, 43). Consistent with these data, CAMA1 cells transfected with FGFR1 harboring the TMD of FGFR4 showed a reduction in both nuclear soluble and chromatin-bound FGFR1 relative to CAMA1 cells transfected with wild type FGFR1 (Fig. 2E).

Cell surface biotinylation assays show that nuclear FGFR1 can also originate from the cell surface (44), suggesting FGFR1 is internalized and traffics to the nucleus via endosomal pathways. Indeed, FGFR1 and FGFR2 can translocate to the nucleus following ligand stimulation in pancreatic stellate cells; this process requires the interaction of FGFR1 with nuclear import proteins, like importin β (15, 45). Once in the nucleus, FGFR1 has been shown to regulate gene transcription (16, 19, 39, 42). Nuclear targeting of FGFR1 by substituting its signal peptide for a nuclear localization sequence (NLS) is sufficient to initiate DNA synthesis and transcription of c-Jun, an activator of cyclin D1. Removal of the kinase region of nuclear-targeted FGFR1 ablates this effect (46). These data suggest the TK function of FGFR1 is necessary for its transcriptional role, consistent with our data from ER+/*FGFR1*-amplified breast cancer cells shown herein.

In summary, we have identified a mechanism by which amplified *FGFR1* can sustain an estrogen-independent tumorigenic population. We propose this mechanism explains, in part, the limited effects of estrogen deprivation on ER+/ *FGFR1*-amplified breast cancers in the clinical trial with letrozole. Based on these data, we propose combinations of ERα and FGFR antagonists should be tested in patients with ER+/*FGFR1*-amplified breast cancer.

## REFERENCES


1. Courjal F, Cuny M, Simony-Lafontaine J, Louason G, Speiser P, Zeillinger R, et al. Mapping of DNA amplifications at 15 chromosomal localizations in 1875 breast tumors: definition of phenotypic groups. Cancer Res. 1997;57(19):4360-7.
2. Jacquemier J, Adelaide J, Parc P, Penault-Llorca F, Planche J, deLapeyriere O, et al. Expression of the FGFR1 gene in human breast-carcinoma cells. Int J Cancer. 1994;59(3):373-8.
3. Reis-Filho JS, Simpson PT, Turner NC, Lambros MB, Jones C, Mackay A, et al. FGFR1 emerges as a potential therapeutic target for lobular breast carcinomas. Clin Cancer Res. 2006;12(22):6652-62.
4. Gorringe KL, Jacobs S, Thompson ER, Sridhar A, Qiu W, Choong DY, et al. High-resolution single nucleotide polymorphism array analysis of epithelial ovarian cancer reveals numerous microdeletions and amplifications. Clin Cancer Res. 2007;13(16):4731-9.
5. Simon R, Richter J, Wagner U, Fijan A, Bruderer J, Schmid U, et al. High-throughput tissue microarray analysis of 3p25 (RAF1) and 8p12 (FGFR1) copy number alterations in urinary bladder cancer. Cancer Res. 2001;61(11):4514-9.
6. Missiaglia E, Selfe J, Hamdi M, Williamson D, Schaaf G, Fang C, et al. Genomic imbalances in rhabdomyosarcoma cell lines affect expression of genes frequently altered in primary tumors: an approach to identify candidate genes involved in tumor development. Genes Chromosomes Cancer. 2009;48(6):455-67.
7. Jiang T, Gao G, Fan G, Li M, Zhou C. FGFR1 amplification in lung squamous cell carcinoma: a systematic review with meta-analysis. Lung Cancer. 2015;87(1):1-7.
8. Turner N, Pearson A, Sharpe R, Lambros M, Geyer F, Lopez-Garcia MA, et al. FGFR1 amplification drives endocrine therapy resistance and is a therapeutic target in breast cancer. Cancer research. 2010;70(5):2085-94.
9. Schlessinger J, Plotnikov AN, Ibrahimi OA, Eliseenkova AV, Yeh BK, Yayon A, et al. Crystal structure of a ternary FGF-FGFR-heparin complex reveals a dual role for heparin in FGFR binding and dimerization. Mol Cell. 2000;6(3):743-50.
10. Turner N, Grose R. Fibroblast growth factor signalling: from development to cancer. Nat Rev Cancer. 2010;10(2):116-29.
11. Bryant DM, Stow JL. Nuclear translocation of cell-surface receptors: lessons from fibroblast growth factor. Traffic. 2005;6(10):947-54.
12. Zammit C, Barnard R, Gomm J, Coope R, Shousha S, Coombes C, et al. Altered intracellular localization of fibroblast growth factor receptor 3 in human breast cancer. J Pathol. 2001;194(1):27-34.
13. Cerliani JP, Guillardoy T, Giulianelli S, Vaque JP, Gutkind JS, Vanzulli SI, et al. Interaction between FGFR-2, STAT5, and progesterone receptors in breast cancer. Cancer Res. 2011;71(10):3720-31.
14. Stachowiak MK, Birkaya B, Aletta JM, Narla ST, Benson CA, Decker B, et al. "Nuclear FGF receptor-1 and CREB binding protein: an integrative signaling module". J Cell Physiol. 2015;230(5):989-1002.
15. Coleman SJ, Chioni AM, Ghallab M, Anderson RK, Lemoine NR, Kocher HM, et al. Nuclear translocation of FGFR1 and FGF2 in pancreatic stellate cells facilitates pancreatic cancer cell invasion. EMBO Mol Med. 2014;6(4):467-81.
16. Chioni AM, Grose R. FGFR1 cleavage and nuclear translocation regulates breast cancer cell behavior. J Cell Biol. 2012;197(6):801-17.
17. Myers JM, Martins GG, Ostrowski J, Stachowiak MK. Nuclear trafficking of FGFR1: a role for the transmembrane domain. J Cell Biochem. 2003;88(6):1273-91.
18. Stachowiak MK, Fang X, Myers JM, Dunham SM, Berezney R, Maher PA, et al. Integrative nuclear FGFR1 signaling (INFS) as a part of a universal "feed-forward-and-gate" signaling module that controls cell growth and differentiation. Journal of cellular biochemistry. 2003;90(4):662-91.
19. Terranova C, Narla ST, Lee YW, Bard J, Parikh A, Stachowiak EK, et al. Global Developmental Gene Programing Involves a Nuclear Form of Fibroblast Growth Factor Receptor-1 (FGFR1). PLoS One. 2015;10(4):e0123380.
20. Katoh M. WNT and FGF gene clusters (review). Int J Oncol. 2002;21(6):1269-73.
21. Brady N, Chuntova P, Bade LK, Schwertfeger KL. The FGF/FGFR axis as a therapeutic target in breast cancer. Expert Rev Endocrinol Metab. 2013;8(4):391-402.
22. Cuny M, Kramar A, Courjal F, Johannsdottir V, Iacopetta B, Fontaine H, et al. Relating genotype and phenotype in breast cancer: an analysis of the prognostic significance of amplification at eight different genes or loci and of p53 mutations. Cancer Res. 2000;60(4):1077-83.
23. Balko JM, Mayer IA, Sanders ME, Miller TW, Kuba MG, Meszoely IM, et al. Discordant cellular response to presurgical letrozole in bilateral synchronous ER+ breast cancers with a KRAS mutation or FGFR1 gene amplification. Molecular cancer therapeutics. 2012;11(10):2301-5.
24. Allred DC, Harvey JM, Berardo M, Clark GM. Prognostic and predictive factors in breast cancer by immunohistochemical analysis. Mod Pathol. 1998;11(2):155-68.
25. Miller TW, Balko JM, Fox EM, Ghazoui Z, Dunbier A, Anderson H, et al. ER alpha-Dependent E2F Transcription Can Mediate Resistance to Estrogen Deprivation in Human Breast Cancer. Cancer Discovery. 2011;1(4):338-51.

26. Debnath J, Muthuswamy SK, Brugge JS. Morphogenesis and oncogenesis of MCF-10A mammary epithelial acini grown in three-dimensional basement membrane cultures. Methods. 2003;30(3):256-68.
27. Bhola NE, Jansen VM, Bafna S, Giltnane JM, Balko JM, Estrada MV, et al. Kinome-wide functional screen identifies role of PLK1 in hormone-independent, ER-positive breast cancer. Cancer Res. 2015;75(2):405-14.
28. Kim D, Pertea G, Trapnell C, Pimentel H, Kelley R, Salzberg SL. TopHat2: accurate alignment of transcriptomes in the presence of insertions, deletions and gene fusions. Genome biology. 2013;14(4):R36.
29. DeLuca DS, Levin JZ, Sivachenko A, Fennell T, Nazaire MD, Williams C, et al. RNA-SeQC: RNA-seq metrics for quality control and process optimization. Bioinformatics. 2012;28(11):1530-2.
30. Miller TW, Hennessy BT, Gonzalez-Angulo AM, Fox EM, Mills GB, Chen H, et al. Hyperactivation of phosphatidylinositol-3 kinase promotes escape from hormone dependence in estrogen receptor-positive human breast cancer. J Clin Invest. 2010;120(7):2406-13.
31. Dowsett M, Smith IE, Ebbs SR, Dixon JM, Skene A, A'Hern R, et al. Prognostic value of Ki67 expression after short-term presurgical endocrine therapy for primary breast cancer. J Natl Cancer Inst. 2007;99(2):167-70.
32. Dixon JM, Renshaw L, Young O, Murray J, Macaskill EJ, McHugh M, et al. Letrozole suppresses plasma estradiol and estrone sulphate more completely than anastrozole in postmenopausal women with breast cancer. J Clin Oncol. 2008;26(10):1671-6.
33. Wolff B, Sanglier JJ, Wang Y. Leptomycin B is an inhibitor of nuclear export: Inhibition of nucleo-cytoplasmic translocation of the human immunodeficiency virus type 1 (HIV-1) Rev protein and Rev-dependent mRNA. Chem Biol. 1997;4(2):139-47.
34. Kwek SS, Roy R, Zhou H, Climent J, Martinez-Climent JA, Fridlyand J, et al. Co-amplified genes at 8p12 and 11q13 in breast tumors cooperate with two major pathways in oncogenesis. Oncogene. 2009;28(17):1892-903.
35. Gao J, Aksoy BA, Dogrusoz U, Dresdner G, Gross B, Sumer SO, et al. Integrative analysis of complex cancer genomics and clinical profiles using the cBioPortal. Sci Signal. 2013;6(269):pl1.
36. Cerami E, Gao J, Dogrusoz U, Gross BE, Sumer SO, Aksoy BA, et al. The cBio cancer genomics portal: an open platform for exploring multidimensional cancer genomics data. Cancer Discov. 2012;2(5):401-4.
37. Gyorffy B, Lanczky A, Eklund AC, Denkert C, Budczies J, Li Q, et al. An online survival analysis tool to rapidly assess the effect of 22,277 genes on breast cancer prognosis using microarray data of 1,809 patients. Breast Cancer Res Treat. 2010;123(3):725-31.
38. Bello E, Colella G, Scarlato V, Oliva P, Berndt A, Valbusa G, et al. E-3810 is a potent dual inhibitor of VEGFR and FGFR that exerts antitumor activity in multiple preclinical models. Cancer Res. 2011;71(4):1396-405.
39. Dunham-Ems SM, Lee YW, Stachowiak EK, Pudavar H, Claus P, Prasad PN, et al. Fibroblast growth factor receptor-1 (FGFR1) nuclear dynamics reveal a novel mechanism in transcription control. Mol Biol Cell. 2009;20(9):2401-12.
40. Sosa LD, Gutierrez S, Petiti JP, Vaca AM, De Paul AL, Torres AI. Cooperative effect of E-2 and FGF2 on lactotroph proliferation triggered by signaling initiated at the plasma membrane. Am J Physiol-Endoc M. 2013;305(1):E41-E9.
41. Liu PCC, Wu LX, Koblish H, Bowman K, Zhang Y, Klabe R, et al. Preclinical characterization of the selective FGFR inhibitor INCB054828. Cancer Research. 2015;75.
42. Somanathan S, Stachowiak EK, Siegel AJ, Stachowiak MK, Berezney R. Nuclear matrix bound fibroblast growth factor receptor is associated with splicing factor rich and transcriptionally active nuclear speckles. J Cell Biochem. 2003;90(4):856-69.
43. Romisch K. Surfing the Sec61 channel: bidirectional protein translocation across the ER membrane. J Cell Sci. 1999;112 ( Pt 23):4185-91.
44. Bryant DM, Wylie FG, Stow JL. Regulation of endocytosis, nuclear translocation, and signaling of fibroblast growth factor receptor 1 by E-cadherin. Mol Biol Cell. 2005;16(1):14-23.
45. Reilly JF, Maher PA. Importin beta-mediated nuclear import of fibroblast growth factor receptor: role in cell proliferation. J Cell Biol. 2001;152(6):1307-12.
46. Wiedlocha A, Falnes PO, Madshus IH, Sandvig K, Olsnes S. Dual mode of signal transduction by externally added acidic fibroblast growth factor. Cell. 1994;76(6):1039-51.

**Figure Legends**

**Figure 1. *FGFR1* amplification and overexpression associate with endocrine resistance in ER+ breast cancer. A**, Clinical trial schema: Patients with stage I-III, ER+/HER2– breast cancer were treated with letrozole for 10-21 days. Surgery was performed following treatment and tumor response was categorized by calculating the natural log (ln) of the post-letrozole Ki67 score as determined by IHC analysis. **B**, *FGFR1* amplification, determined by FISH, was significantly associated with resistant vs. intermediate or sensitive tumors ($p<0.05$, Fisher's t-test). **C-E**, Tumor sections were stained for FGFR; the percent of FGFR1-positive tumor cells and staining intensity were assessed in both the cytoplasmic and nuclear compartments by a blinded expert breast pathologist (M.V.E.) to generate a H-score (**D**). The percent of cytoplasmic and nuclear FGFR1+ tumor cells and their staining intensity were assessed by a blinded expert pathologist (M.V.E.) to generate a H-score. Total and nuclear FGFR1 H-scores are shown in **C** and **E**, respectively (Fisher's t-test). Both total and nuclear FGFR1 staining was higher in post-treatment tumor sections.

**Figure 2. Estrogen deprivation increases nuclear and cytosolic FGFR1 expression. A,** Immunoblot analysis of lysates from CAMA1, HCC1500 and MDA-MB-134 cells exposed to short-term estrogen deprivation up to 6 days revealed an increase in FGFR1 expression over time. HCC1500 cells showed increased expression of the cleaved form of FGFR1. **B,** Immunoblot analysis of parental and LTED ER+ cell lines following 24 h of estrogen deprivation revealed an increase in FGFR1 and ERα in *FGFR1*-amplified $CAMA1^{LTED}$ and $MDA\text{-}MB\text{-}134^{LTED}$ cells but not in *FGFR1* non-amplified MCF-7 cells. **C,** Proximity ligation assay (PLA) to detect FGFR1 expression. Analysis of red, amplified loci by confocal microscopy confirmed immunoblot and FISH results in that $CAMA1^{LTED}$ cells harbor more cytosolic and nuclear FGFR1 compared to CAMA1 parental cells. Each bar in the graph to the right of the PLA image represents the mean nuclear fluorescent signals ± SD of 3 wells. **D,** CAMA1 cells stably transduced with constructs encoding wild-type FGFR1 ($CAMA1^{FGFR1}$) or FGFR1 in which the TMD has been substituted with the FGFR4 TMD ($CAMA1^{FGFR1/TMD\text{-}FGFR4}$) were lysed for immunoblot analysis with FGFR and tubulin antibodies. **E,**

Membrane, cytoplasmic, nuclear soluble and chromatin-bound fractions of CAMA$^{FGFR1}$ and CAMA$^{FGFR1/TMD-FGFR4}$ cells demonstrates that substitution of the FGFR1 TMD with the TMD of FGFR4 reduces detectable nuclear FGFR1, particularly the chromatin-bound fraction in CAMA1$^{FGFR1/TMD-FGFR4}$ cells compared to CAMA1$^{FGFR1}$ cells. Apoptosis-inducing factor (AIF), tubulin, lamin A/C and histone H1 antibodies were used as controls for the cell fractionation. **F,** Immunofluorescence (IF) was performed in CAMA1 cells treated with vehicle or 30 ng/mL leptomycin B for 2 h. Nuclear localization of FGFR1 was detected by confocal microscopy. Each bar represents the mean nuclear fluorescent signals ± SD of 3 wells.

**Figure 3. FGF3/4/19 expression is upregulated upon estrogen deprivation. A**, FISH analysis of primary tumor sections showed co-amplification of *FGFR1* and *11q12-14* mainly in letrozole-resistant vs. intermediate and sensitive cancers (p=0.0001, Fisher's t-test). **B**, Co-amplification of *11q12-14* was observed in ER+/*FGFR1*-amplified cell lines MDA-MB-134, CAMA1 and HCC1500; the Y axis shows the 11q12-14:Chr.11 ratio. **C**, Relative transcript expression of FGF3/4/19 in the indicated cell lines was determined by qPCR as described in Methods. **D**, Transcript levels of FGF3/4/19 were higher in *FGFR1*-amplified LTED cells (CAMA1 and MDA-MB-134) but not in *FGFR1* non-amplified MCF-7$^{LTED}$ cells compared to their parental counterparts (Fisher's t-test). **E**, CAMA1 cells were treated with 100 ng/mL FGF3 ± 2 μM lucitanib in estrogen-free medium. After 15 days, plates were washed and stained with crystal violet and their imaging intensity was quantified by spectrophotometric detection. Representative images and quantification of the integrated intensity values as % of vehicle-treated controls are shown (Fisher's t-test). **F,** CAMA1 cells were plated in 100-mm dishes and transfected with FGFR1 or control siRNAs as described in Methods. Medium containing 100 ng/mL FGF3 was replenished every 3 days. Seven days later, monolayers were harvested and cell counts determined using a Coulter Counter. Each bar in the left panel represents the mean cell number ± SD of triplicate wells (Fisher's t-test). FGFR1 knockdown was confirmed by immunoblot analysis of cell lysates from plates treated identically in parallel (right panel).

**Figure 4. Long-term estradiol deprivation increases the interaction of FGFR1 with ERα. A**, FGFR1 was precipitated from MDA-MB-134, CAMA1 and CAMA1$^{LTED}$ cell lysates; immune complexes were separated by SDS-PAGE and subjected to immunoblot analysis with an ERα antibody. CAMA1$^{LTED}$ cells exhibited greater levels of FGFR1-ERα co-immunoprecipitation compared to CAMA1 cells. **B,** FGFR1 was precipitated from CAMA1 and CAMA1$^{LTED}$ nuclear extracts with C-terminal (Abcam) and N-Terminal (Cell Signaling) FGFR1 antibodies; immune complexes were separated by SDS-PAGE and analyzed by ERα immunoblot. **C-D**, PLA of CAMA1$^{LTED}$ cells showed greater nuclear co-localization of FGFR1 and ERα compared to parental CAMA1 cells. PLA foci/cell are quantified in **D. E-F**, CAMA1$^{LTED}$ cells were treated with 2 μM lucitanib or 1 μM fulvestrant for 6 h. Monolayers were subjected to PLA as described in Methods. Quantification of FGFR1-ERα complexes as PLA signals/cell is shown in (**F)**. Each bar represents the mean ± SD of 3 wells. **G-H**, CAMA1 cells were stable transfected with expression vectors encoding GFP, FGFR1 and FGFR1/TK– (K514M TK mutant), as described in Methods, and then plated in chamber slides followed by PLA. Quantification of FGFR1-ERα complexes as PLA signals/cell is shown in (**H**). Each bar represents the mean ± SD of 3 wells. **I-J**, Paired pre- and post-letrozole primary tumor sections were subjected to PLA as described in Methods. Post-letrozole tumor cells exhibited more FGFR1-ERα complexes compared to pre-treatment tumor cells as quantitated in **J**. Each bar represents the mean PLA signals/cell ± SD of 20 cells counted in each of 4 high-power fields.

**Figure 5. Identification of FGF-sensitive ERα and FGFR1 genomic binding sites. A-B**, CAMA1 cells were plated in estrogen-free medium and stimulated with 100 ng/mL FGF3 for 6 h in the presence of 1 μM fulvestrant, 2 μM lucitanib or the combination. Cells were harvested and subjected to ChIP-seq as described in Methods. Shown are heatmaps generated from ChIP-seq analysis of ERα **(A)** and FGFR1 **(B)** DNA binding. Treatment with fulvestrant, lucitanib or the combination reduced binding of ERα (A) or FGFR1 (B) binding to DNA. Heatmaps represent the mean of two different experiments. **C-D**, Heatmaps of ChIP-seq data showing the effects of fulvestrant, lucitanib or the

combination on DNA/ERα-associated (**C**) and DNA/FGFR1-associated (**D**) genes, respectively, as shown in **A-B**. **E-F**, Gene set enrichment analysis (GSEA) of FGFR1- and ERα-associated genes. Numbers to the right of each bar represent the False Discovery Rate (FDR) q-value. **G**, Volcano plot analysis of differentially expressed genes in tumors from patients treated with letrozole in the clinical trial. Each data point represents the ratio of the average expression for a particular gene in *FGFR1*-amplified tumors (n=7) vs. *FGFR1* non-amplified tumors (n=25). The red dots in the Volcano plot represent genes that are significantly up- or down-regulated >2-fold with $p<0.01$. **H**, GSEA of significantly enriched genes in *FGFR1*-amplified relative to *FGFR1* non-amplified tumors showed that ERα-related pathways are still active in estrogen-deprived (by letrozole treatment) ER+/*FGFR1*-amplified primary tumors **(G)**. Numbers to the right of each bar represent the FDR q-value.

**Figure 6. Treatment with FGFs induces expression of ERα-dependent genes. A,** CAMA1 cells were plated in estrogen-free medium and treated with 100 ng/mL FGF3/19 for 6 h. At this time, cells were harvested and RNA prepared and analyzed for mRNA expression changes in ERα pathway genes using the $RT^2$ Profiler Estrogen Receptor Signaling PCR Array (Qiagen). **B-C**, *CCND1*, *EGR3* and *THSB1* mRNA expression was confirmed by qRT-PCR in CAMA1 cells treated with FGF3 (**B**) or FGF19 (**C**) for 6 h ± 2 μM lucitanib or 1 μM fulvestrant. Each bar represents the mean *CCND1*, *EGR3* and *THSB1* transcript levels ± SD (Fisher's t-test).

**Figure 7. Combined blockade of FGFR1 and ERα potently inhibits growth of ER+/*FGFR1*-amplified breast cancers. A-B,** CAMA1 cells were cultured in 3D Matrigel as described in Methods and treated with vehicle, 2 μM lucitanib, 1 μM fulvestrant or the combination. After 15 days, images were captured from 3 different fields using a CK40 microscope. Quantitation of representative images is shown in (**B**). Each bar represents the fold change in colony number relative to vehicle ± SD of three replicate wells repeated twice (Fisher's t-test). **C,** CAMA1 cells in were treated as in A & B for 6 h, after which lysates were prepared and subjected to immunoblot analyses with the indicated antibodies. **E,** ER+/HER2–/*FGFR1*-amplified TM00368 PDXs were established in ovariectomized SCID/beige mice implanted with a s.c. 21-day relase, 0.25-mg 17β-estradiol pellet.

Once tumors reached ≥200 $mm^3$, mice were randomized to treatment with vehicle, fulvestrant (5 mg/kg/week), lucitanib (7 mg/kg/day), or both drugs for 3 weeks. Each data point represents the mean tumor volume in $mm^3$ ± SD (n=8 per arm; ANOVA test). **F,** Bar graph showing the % change in volume in individual TM00368 PDXs after three weeks of treatment relative to tumor volumes on day 0 (baseline). **G-H,** TM00368 tumors were harvested at the end of treatment. FFPE tumor sections were prepared and subjected to IHC with Y653/4 phosphorylated FGFR1 and ERα antibodies as described in Methods. The percent of phospho-FGFR1+ and ER+ tumor cells and their staining intensity was assessed by an expert breast pathologist (M.V.E.) blinded to treatment to generate an H-score. Nuclear phospho-FGFR1 and ERα H-scores are shown Fisher's t-test). **I,** FGFR1 was precipitated from lysates of TM00368 tumors harvested at the end of treatment; immune complexes were separated by SDS-PAGE and subjected to immunoblot analysis with the indicated antibodies. Bottom two lanes show FGFR1 and ERα content in lysates before i.p.

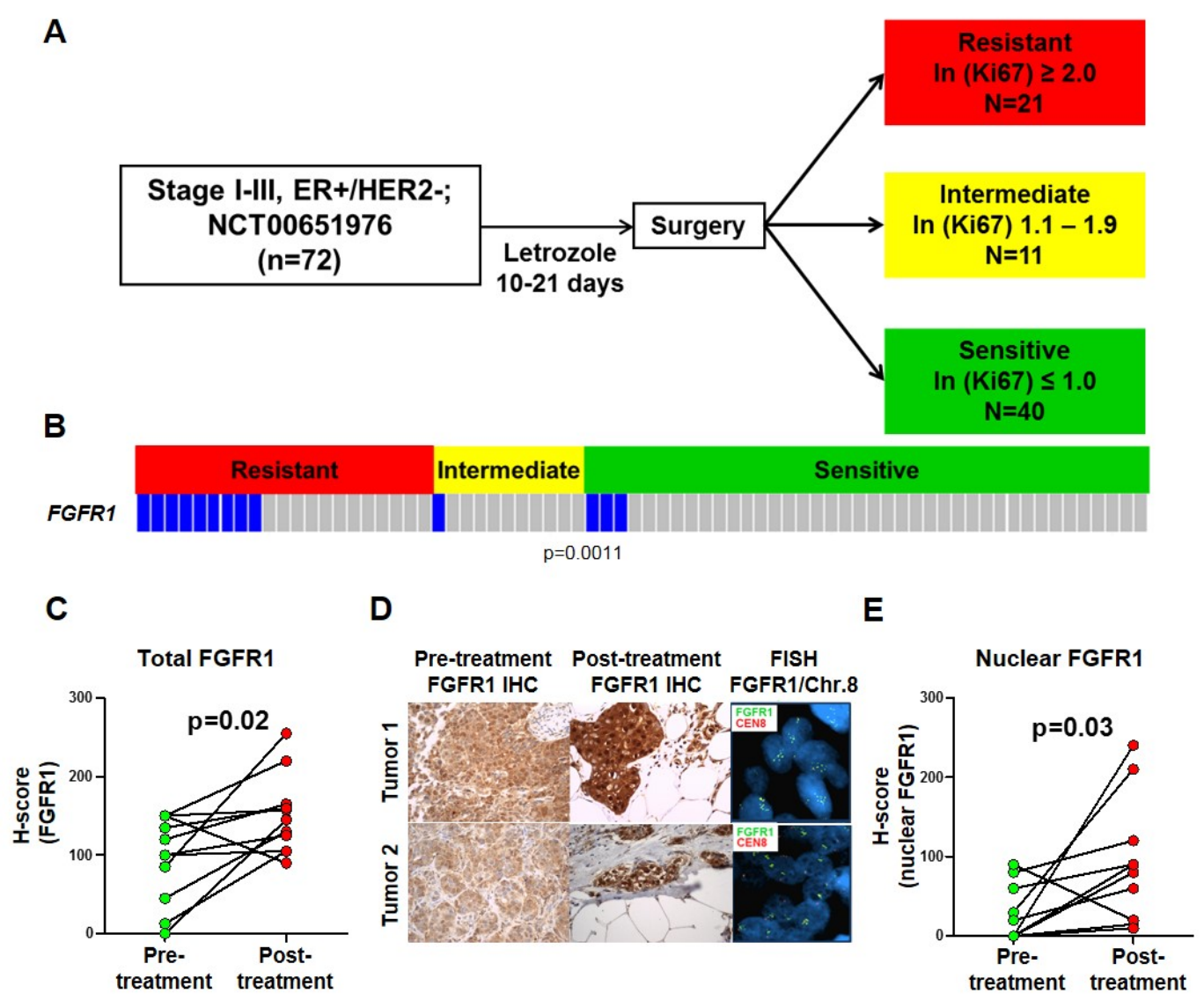
A
Stage I-III, ER+/HER2-;
NCT00651976
(n=72)
Letrozole
10-21 days
Surgery
Resistant
ln (Ki67) ≥ 2.0
N=21
Intermediate
ln (Ki67) 1.1 – 1.9
N=11
Sensitive
ln (Ki67) ≤ 1.0
N=40
B
Resistant
Intermediate
Sensitive
FGFR1
p=0.0011
C
Total FGFR1
p=0.02
H-score
(FGFR1)
300
200
100
0
Pre-
treatment
Post-
treatment
D
Pre-treatment
FGFR1 IHC
Post-treatment
FGFR1 IHC
FISH
FGFR1/Chr.8
Tumor 1
Tumor 2
FGFR1
CEN8
E
Nuclear FGFR1
p=0.03
H-score
(nuclear FGFR1)
300
200
100
0
Pre-
treatment
Post-
treatment

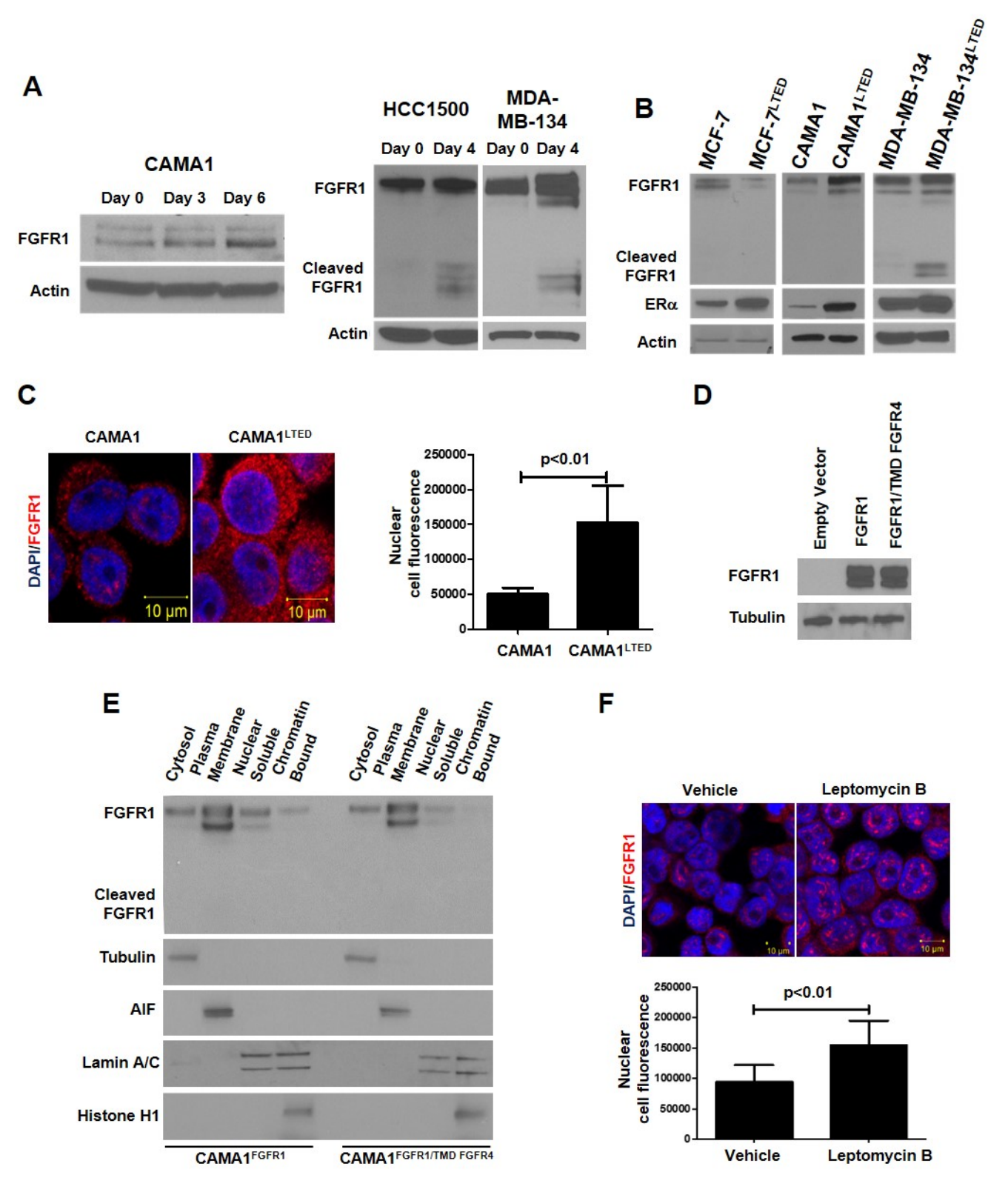
A
CAMA1
Day 0
Day 3
Day 6
FGFR1
Actin
HCC1500
MDA-MB-134
Day 0
Day 4
Day 0
Day 4
FGFR1
Cleaved FGFR1
Actin
B
MCF-7
MCF-7LTED
CAMA1
CAMA1LTED
MDA-MB-134
MDA-MB-134LTED
FGFR1
Cleaved FGFR1
ERα
Actin
C
CAMA1
CAMA1LTED
DAPI/FGFR1
10 μm
10 μm
Nuclear cell fluorescence
250000
200000
150000
100000
50000
0
p<0.01
CAMA1
CAMA1LTED
D
Empty Vector
FGFR1
FGFR1/TMD FGFR4
FGFR1
Tubulin
E
Cytosol
Plasma Membrane
Nuclear Soluble
Chromatin Bound
Cytosol
Plasma Membrane
Nuclear Soluble
Chromatin Bound
FGFR1
Cleaved FGFR1
Tubulin
AIF
Lamin A/C
Histone H1
CAMA1FGFR1
CAMA1FGFR1/TMD FGFR4
F
Vehicle
Leptomycin B
DAPI/FGFR1
10 μm
10 μm
Nuclear cell fluorescence
250000
200000
150000
100000
50000
0
p<0.01
Vehicle
Leptomycin B

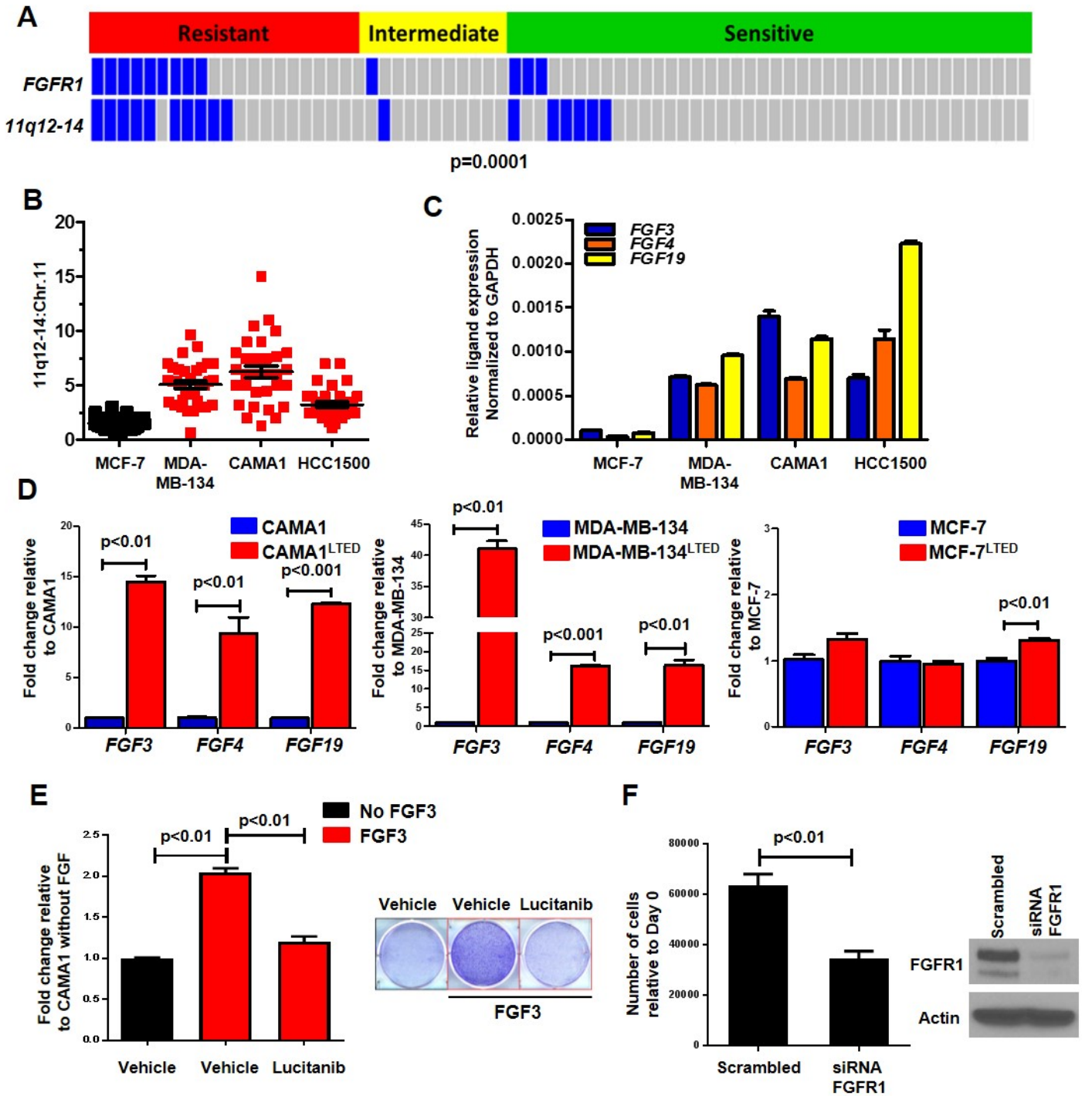
A
Resistant
Intermediate
Sensitive
FGFR1
11q12-14
p=0.0001
B
11q12-14:Chr.11
MCF-7
MDA-MB-134
CAMA1
HCC1500
C
Relative ligand expression Normalized to GAPDH
FGF3
FGF4
FGF19
D
Fold change relative to CAMA1
CAMA1
CAMA1LTED
p<0.01
p<0.001
Fold change relative to MDA-MB-134
MDA-MB-134
MDA-MB-134LTED
Fold change relative to MCF-7
MCF-7
MCF-7LTED
E
Fold change relative to CAMA1 without FGF
No FGF3
FGF3
Vehicle
Lucitanib
F
Number of cells relative to Day 0
Scrambled
siRNA FGFR1
FGFR1
Actin

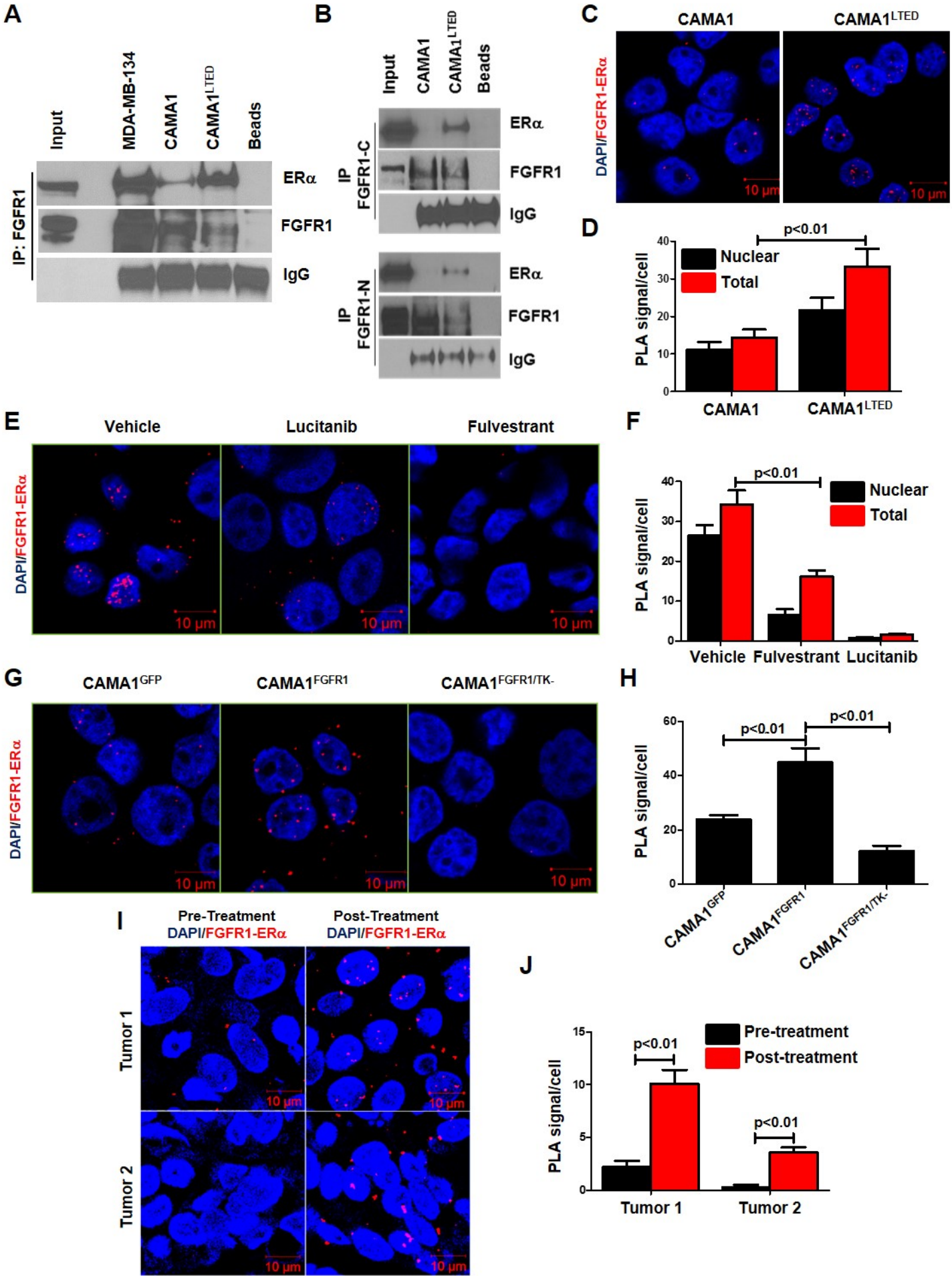
A
Input
MDA-MB-134
CAMA1
CAMA1LTED
Beads
IP: FGFR1
ERα
FGFR1
IgG
B
Input
CAMA1
CAMA1LTED
Beads
IP FGFR1-C
IP FGFR1-N
ERα
FGFR1
IgG
C
CAMA1
CAMA1LTED
DAPI/FGFR1-ERα
10 μm
D
p<0.01
Nuclear
Total
PLA signal/cell
CAMA1
CAMA1LTED
E
Vehicle
Lucitanib
Fulvestrant
DAPI/FGFR1-ERα
10 μm
F
p<0.01
Nuclear
Total
PLA signal/cell
Vehicle
Fulvestrant
Lucitanib
G
CAMA1GFP
CAMA1FGFR1
CAMA1FGFR1/TK-
DAPI/FGFR1-ERα
10 μm
H
p<0.01
p<0.01
PLA signal/cell
CAMA1GFP
CAMA1FGFR1
CAMA1FGFR1/TK-
I
Pre-Treatment
DAPI/FGFR1-ERα
Post-Treatment
DAPI/FGFR1-ERα
Tumor 1
Tumor 2
10 μm
J
p<0.01
p<0.01
Pre-treatment
Post-treatment
PLA signal/cell
Tumor 1
Tumor 2

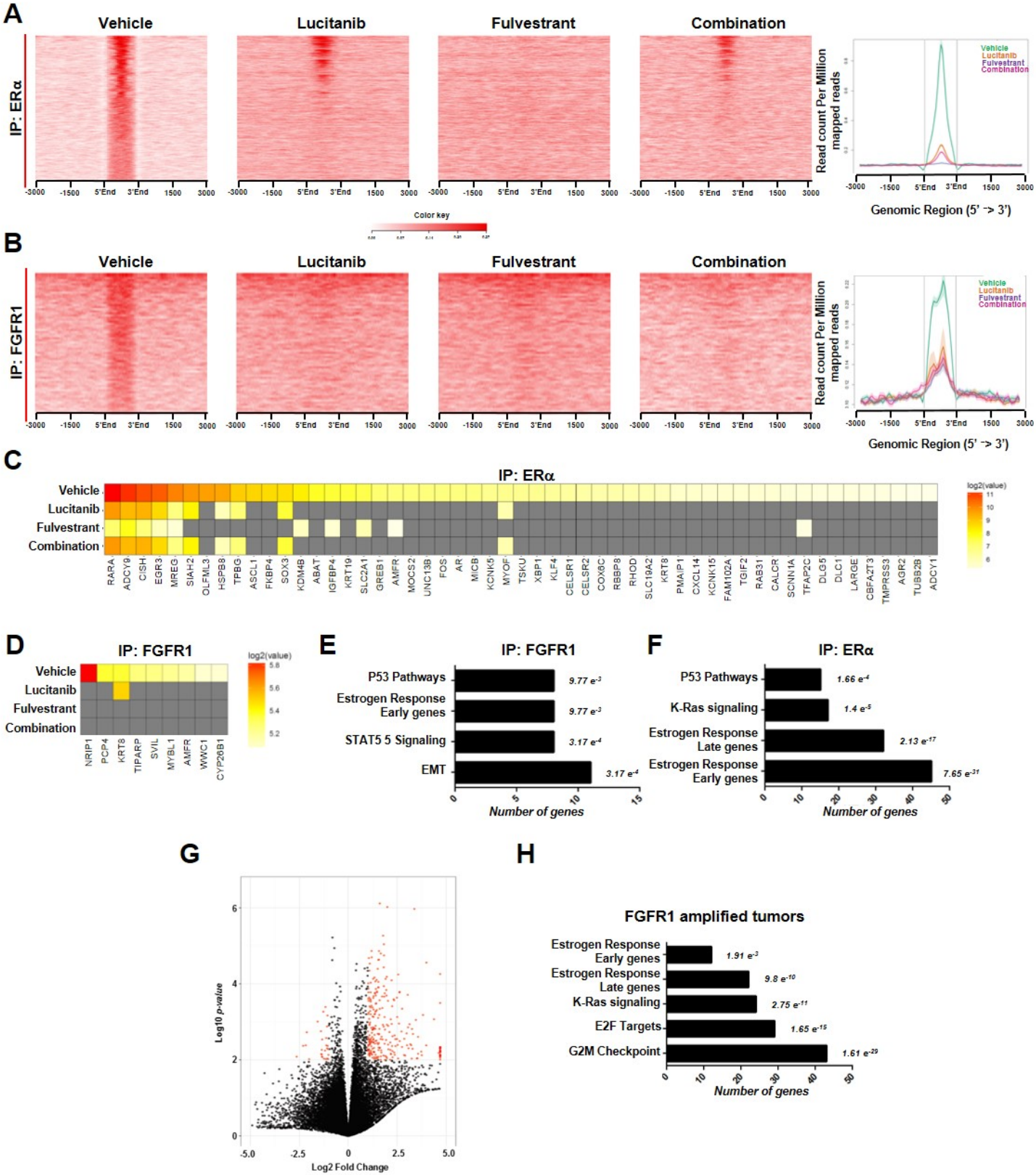
A
Vehicle
Lucitanib
Fulvestrant
Combination
IP: ERα
Read count Per Million mapped reads
Genomic Region (5' -> 3')
Color key
B
IP: FGFR1
C
IP: ERα
log2(value)
D
IP: FGFR1
E
IP: FGFR1
P53 Pathways
Estrogen Response Early genes
STAT5 5 Signaling
EMT
Number of genes
F
IP: ERα
P53 Pathways
K-Ras signaling
Estrogen Response Late genes
Estrogen Response Early genes
Number of genes
G
Log10 p-value
Log2 Fold Change
H
FGFR1 amplified tumors
Estrogen Response Early genes
Estrogen Response Late genes
K-Ras signaling
E2F Targets
G2M Checkpoint
Number of genes

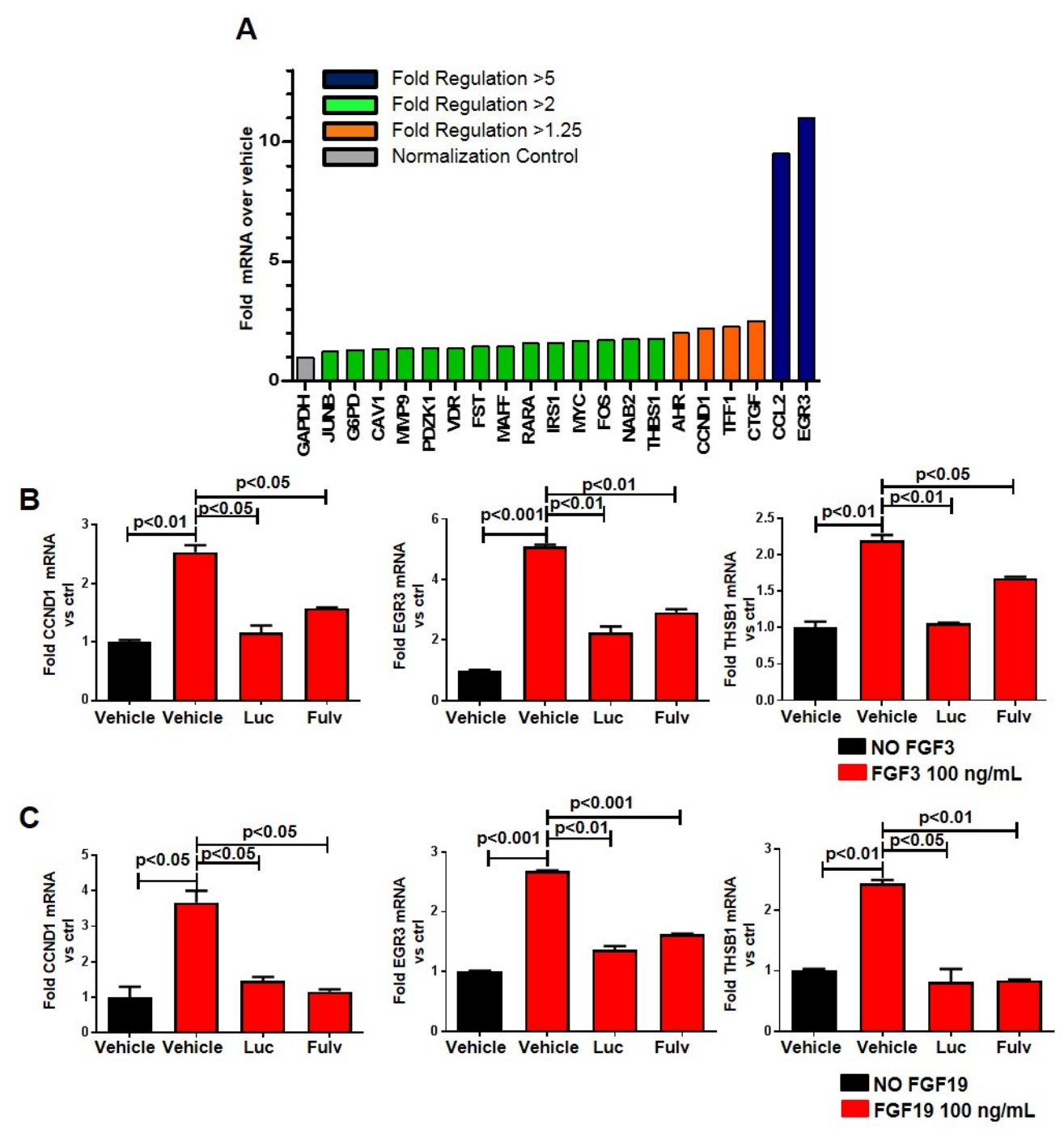
A
Fold Regulation >5
Fold Regulation >2
Fold Regulation >1.25
Normalization Control
Fold mRNA over vehicle
0
5
10
GAPDH
JUNB
G6PD
CAV1
MMP9
PDZK1
VDR
FST
MAFF
RARA
IRS1
MYC
FOS
NAB2
THBS1
AHR
CCND1
TFF1
CTGF
CCL2
EGR3
B
Fold CCND1 mRNA vs ctrl
p<0.01
p<0.05
p<0.05
Vehicle
Vehicle
Luc
Fulv
Fold EGR3 mRNA vs ctrl
p<0.001
p<0.01
p<0.01
Fold THSB1 mRNA vs ctrl
p<0.01
p<0.01
p<0.05
NO FGF3
FGF3 100 ng/mL
C
Fold CCND1 mRNA vs ctrl
p<0.05
p<0.05
p<0.05
Fold EGR3 mRNA vs ctrl
p<0.001
p<0.01
p<0.001
Fold THSB1 mRNA vs ctrl
p<0.01
p<0.05
p<0.01
NO FGF19
FGF19 100 ng/mL

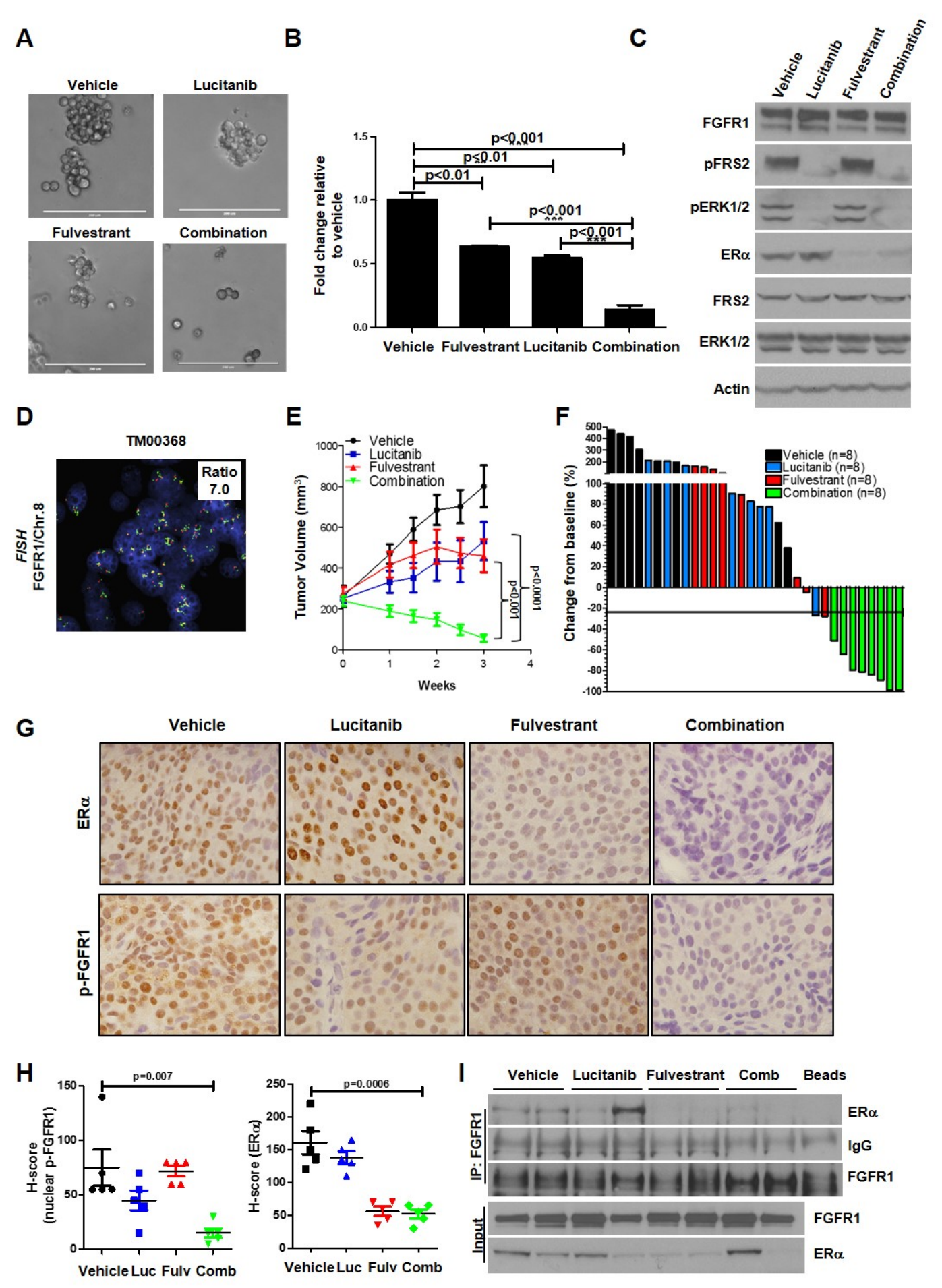
A
Vehicle
Lucitanib
Fulvestrant
Combination
B
Fold change relative to vehicle
p<0.001
p<0.01
p<0.01
p<0.001
p<0.001
Vehicle
Fulvestrant
Lucitanib
Combination
C
Vehicle
Lucitanib
Fulvestrant
Combination
FGFR1
pFRS2
pERK1/2
ERα
FRS2
ERK1/2
Actin
D
TM00368
Ratio 7.0
FISH FGFR1/Chr.8
E
Vehicle
Lucitanib
Fulvestrant
Combination
Tumor Volume (mm3)
Weeks
p<0.0001
p<0.0001
F
Vehicle (n=8)
Lucitanib (n=8)
Fulvestrant (n=8)
Combination (n=8)
Change from baseline (%)
G
Vehicle
Lucitanib
Fulvestrant
Combination
ERα
p-FGFR1
H
p=0.007
H-score (nuclear p-FGFR1)
Vehicle
Luc
Fulv
Comb
p=0.0006
H-score (ERα)
Vehicle
Luc
Fulv
Comb
I
Vehicle
Lucitanib
Fulvestrant
Comb
Beads
IP: FGFR1
ERα
IgG
FGFR1
Input
FGFR1
ERα

## Supplementary Figures

**Supplementary Figure 1. Effect of letrozole on expression and localization of FGFR1 in primary breast tumors without *FGFR1* amplification.** *FGFR1* gene copy number and protein expression were determined by FISH (FGFR1:Chr.8 ratio, 100x magnification) and IHC, respectively. Total (**A**) and nuclear (**B**) FGFR1 expression was decreased in post-letrozole compared to paired pre-letrozole patient tumors (***$p$<0.001 vs. pre-letrozole, Fisher's $t$-test). Representative IHC and FISH images are shown in **B.**

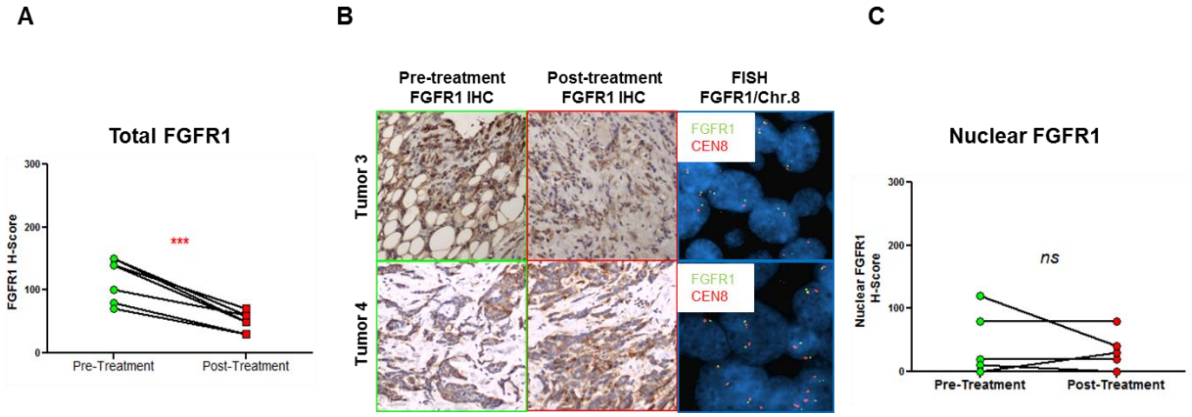

**Supplementary Figure 2**. ***FGFR1*** **amplification and protein expression in ER+ human breast cancer cell lines. A**, Table depicts the *FGFR1:Chr.8* ratio in a panel of ER+ human breast cancer cell lines as determined by FISH. MDA-MB-134, CAMA1, and HCC1500 cells are *FGFR1* amplified, whereas MCF7 and ZR75.1 cells are not. **B,** Immunoblot analysis of cell lysates displays the relative content of the full-length and cleaved forms of FGFR1, FRS2, phosphorylated FRS2 and ERα, using actin as a loading control. **C,** Membrane, cytoplasmic, nuclear and chromatin-bound fractions of CAMA1 cells revealed full-length FGFR1 in both nuclear soluble and chromatin-bound fractions. Apoptosis-inducing factor (AIF), tubulin, lamin A/C and histone H1 antibodies were used as controls. **D,** Immunofluorescence analysis was performed in $CAMA1^{FGFR1}$ cells treated with vehicle or 30 ng/mL leptomycin B for 2 h. Nuclear localization of FGFR1 was detected by confocal microscopy. Each bar represents the mean nuclear fluorescent signals ± SD of 3 wells. **E-F**, PLA was used to assess FGFR1 expression in CAMA1 cells transfected with FGFR1 siRNA or a negative (scrambled) control as described in Methods. Cell lysates from identically-treated parallel plates were prepared and subjected to immunoblot analysis with the indicated antibodies to confirm siRNA-mediated FGFR1 knockdown.

A

| Cell line | Ratio FGFR1:Chr.8 | Status |
|---|---|---|
| MCF7 | 0.77 | *No Amp* |
| ZR75.1 | 1.69 | *No Amp* |
| MDA-MB-134 | 6.8 | *Amp* |
| CAMA1 | 2.31 | *Amp* |
| HCC1500 | 2.03 | *Amp* |

B

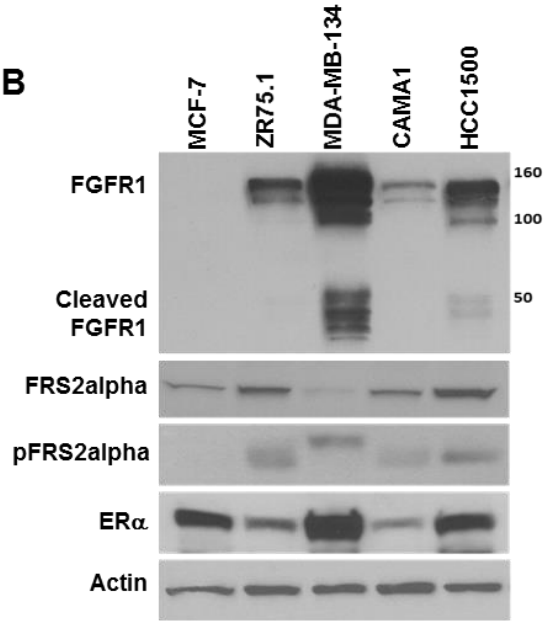


C

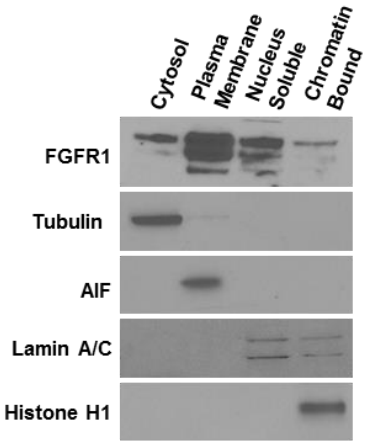


D

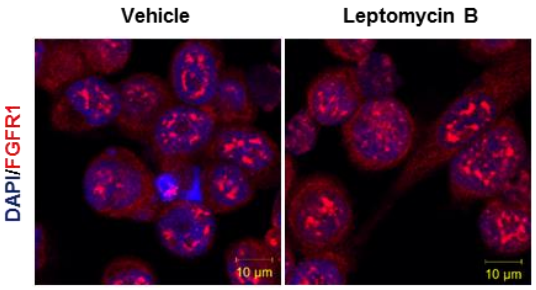


E

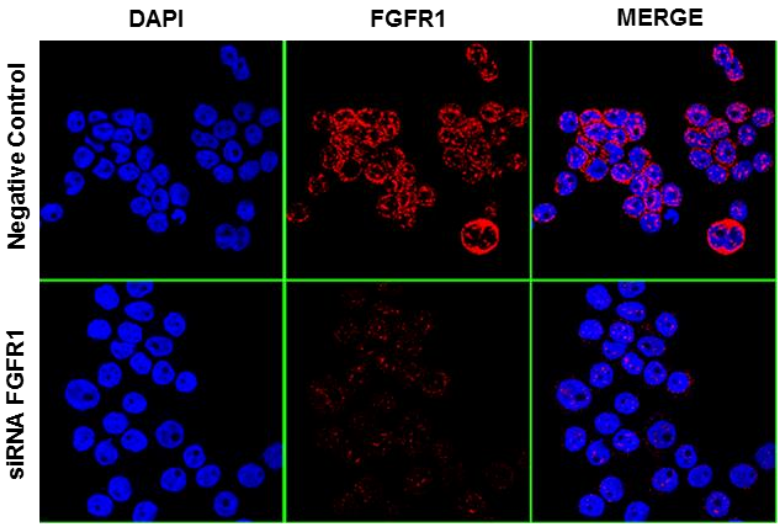


F

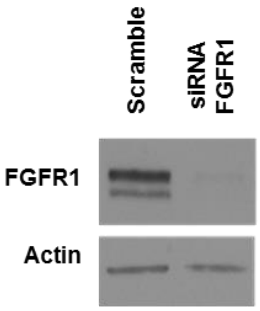

**Supplementary Figure 3. Breast cancers with co-amplification of *FGFR1* and *11q12-14* genes exhibit decreased time to recurrence. A,** Tile plot of ER+ breast cancers in TCGA (Cell 2015) with co-amplification of *FGF3/4/19* and *CCND1* on chr.11q12-14 and of *FGFR1* on chr. 8p11. **B**, Analysis of TCGA breast whole exome sequencing (WES) data showed significant co-occurrence of *FGFR1* and *FGF3/4/19* amplification (n=594 samples; p<0.001, Fisher's *t*-test). **C**, Kaplan Meier plot from the KMPLOT gene expression database showing the probability of relapse for patients with ER+ breast cancer treated with endocrine therapy comparing the high and low tertiles of both *FGFR1* and *FGF3/4/19* mRNA expression by microarray. Patients in the high tertile tended toward a shorter relapse-free survival compared to patients in the low tertile (HR 1.75, $p$ =0.069).

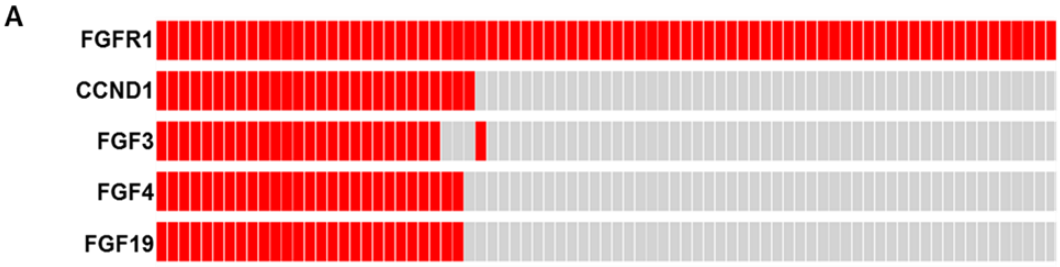


B

| Gene A | Gene B | p-Value | Association |
|---|---|---|---|
| FGFR1 | CCND1 | <0.001 | Tendency towards co-occurrence |
| FGFR1 | FGF3 | <0.001 | Tendency towards co-occurrence |
| FGFR1 | FGF4 | <0.001 | Tendency towards co-occurrence |
| FGFR1 | FGF19 | <0.001 | Tendency towards co-occurrence |

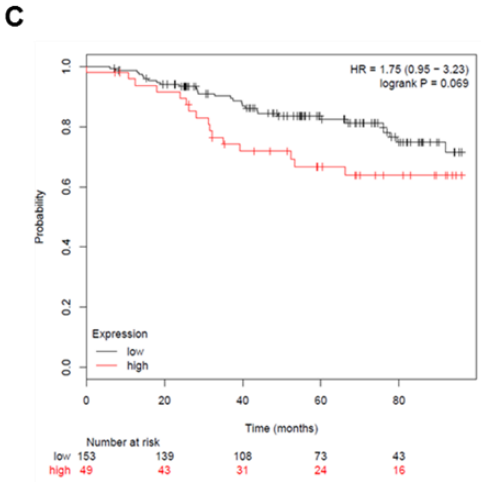

**Supplementary Figure 4. Estrogen deprivation upregulates FGF ligand expression in ER+/*FGFR1*-amplified cells. A,** *11q12-14* amplification was determined in a panel of ER+ cell lines by FISH using *CCND1* and chromosome 11 centromere probes. *FGFR1*-amplified MDA-MB-134, CAMA1, and HCC1500 cell lines exhibited co-amplification at *11q12-14*. **B,** MDA-MB-134, CAMA1 and HCC1500 cells were cultured in full media or estrogen-free medium for 24 h. RNA was collected at that time and subjected to mRNA expression analysis by qPCR as described in Methods. Estrogen-deprivation (grey bars) resulted in an increase in *FGF3/4/19* transcript levels compared to non-deprived conditions (black bars) (*p<0.05 vs. control, Fisher's t-test).

**A**

| Cell line | Ratio 11q12-14:Chr.11 | Status |
|---|---|---|
| MCF7 | 1.9 | *No Amp* |
| MDA134 | 4.9 | *Amp* |
| CAMA1 | 5.4 | *Amp* |
| HCC1500 | 3.0 | *Amp* |

**B**

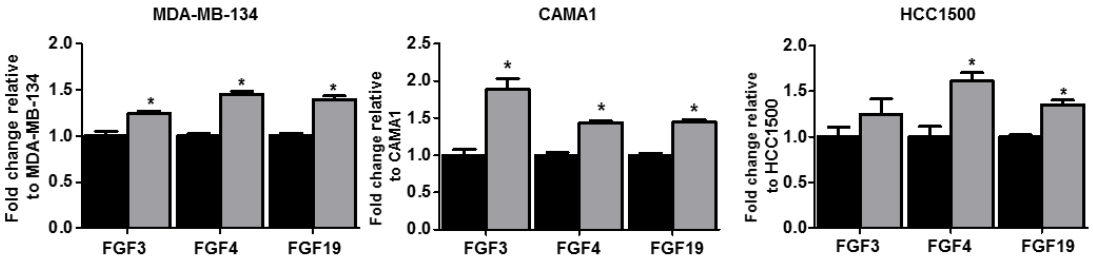

**Supplementary Figure 5. A,** CAMA1$^{GFP}$, CAMA1$^{FGFR1/WT}$ and CAMA1$^{FGFR1/TK–}$ cells were treated with 100 ng/mL FGF3 for 6 h and then lysed for immunoblot analysis with the indicated antibodies. **B-C,** CAMA1$^{GFP}$ and CAMA1$^{FGFR1/TK–}$ cells were seeded in 6-well plates in estrogen-free media. After 14 days, monolayers were stained with crystal violet. Images of the plates were obtained (**B**) and image intensity was quantitated as described in Methods. Quantitation is shown in (**C**; ***$p$<0.001 vs. CAMA1$^{GFP}$, Fisher's $t$-test). **D,** CAMA1$^{GFP}$ ± 2 μM lucitanib and CAMA1$^{FGFR1/TK–}$ cells were plated in estrogen-free medium and treated with 100 ng/mL FGF3 for 6 h. At this time, cells were harvested and RNA was prepared and analyzed for *THBS1, CCND1, CCL2* and *EGR3* mRNA changes by qRT-PCR. Each bar represents the mean transcript level ± SD (*$p$<0.05, **$p$<0.01, ***$p$<0.001 vs. CAMA1$^{GFP}$, Fisher's $t$-test).

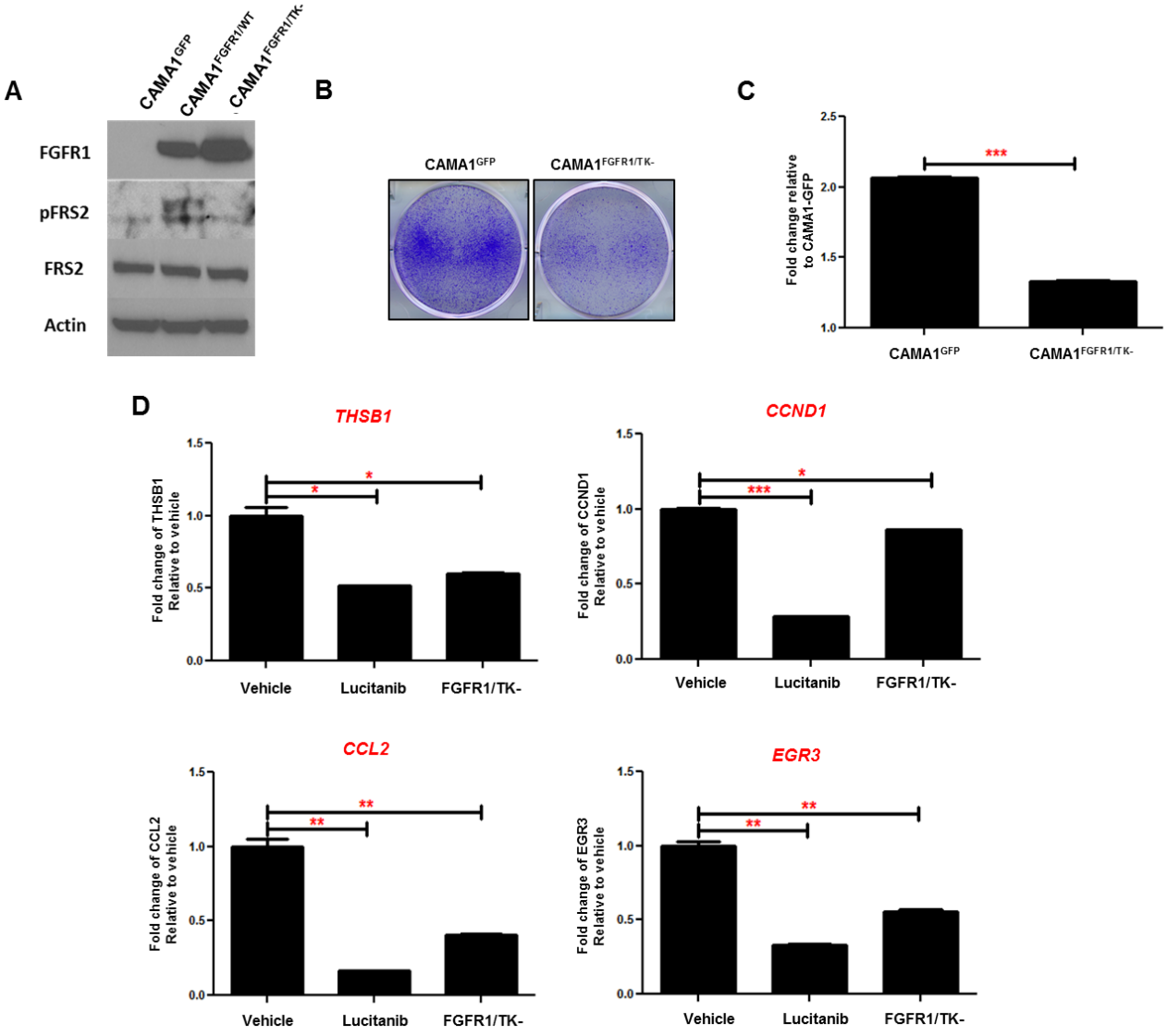

**Supplementary Figure 6. FGFs induce ERα and FGFR1 DNA binding. A-B,** Heatmaps from ChIP-seq analysis of estrogen-deprived CAMA1 cells ± 100 ng/mL FGF3 (6 h) showing ERα (**A**) and FGFR1 (**B**) DNA binding peaks. The heatmaps represent the mean of two different experiments. **C-D**, CAMA1 cells were plated in estrogen-free media and treated with vehicle, 2 μM lucitanib, 1 μM fulvestrant or the combination for 6 h. ChIP was performed with ERα (**C**) or FGFR1 (**D**) antibodies. Primers to amplify FGFR1 or ERα binding regions were used in qPCR to determine fold enrichment relative to input. Two-tailed Student's unpaired t test was performed to compare mean signal amplification in cells treated with vehicle vs. lucitanib plus fulvestrant. Each bar represents the mean fold-enrichment in ERα-ChIP (**C**) or FGFR1-ChIP (**D**) ± SD of two independent experiments with three technical replicates each.

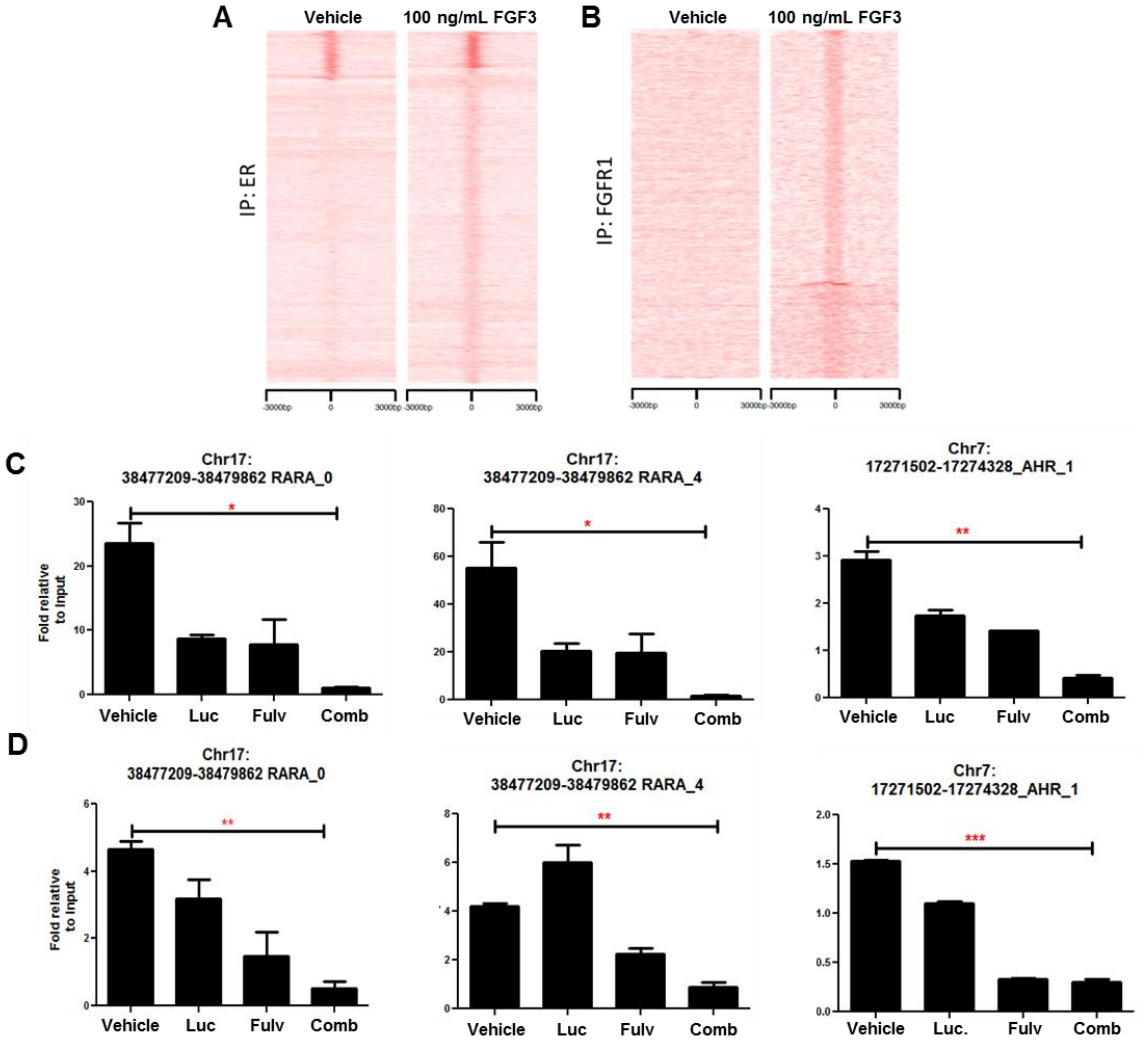

**Supplementary Figure 7. ER+/*FGFR1*-amplified tumors exhibit differential gene expression compared to ER+/*FGFR1* non-amplified breast cancers**. Heatmap of G2M checkpoint genes, E2F target genes and estrogen-response genes identified by Gene Set Enrichment Analysis (GSEA) in ER+/*FGFR1*-amplified vs. ER+/*FGFR1* non-amplified breast tumors from patients treated with letrozole in the clinical trial.

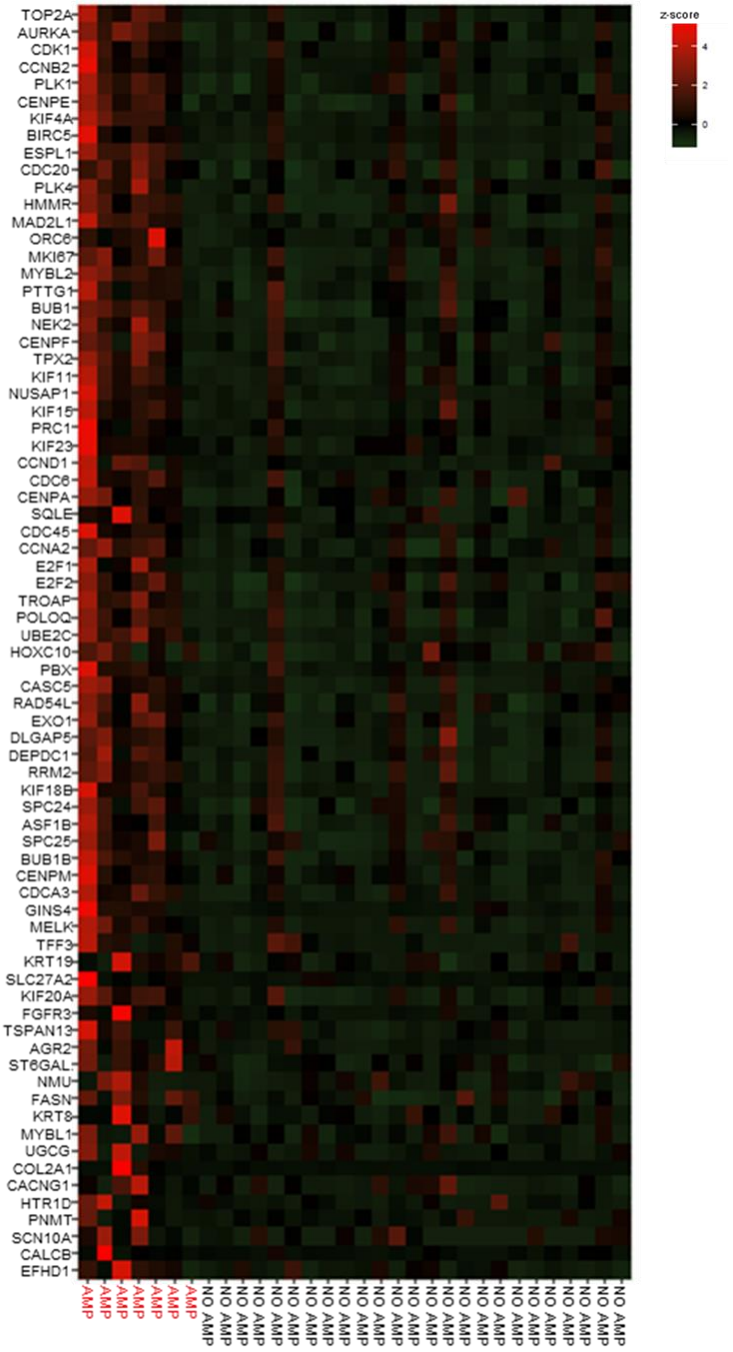

**Supplementary Figure 8. Treatment with FGFs induces expression of ERα-dependent genes.** CAMA1 and CAMA1$^{LTED}$ cells were plated in estrogen-free medium and treated with 100 ng/mL FGF3 for 6 h. At this time, cells were harvested and RNA prepared and analyzed for mRNA expression changes in ERα pathway genes using the RT$^2$ Profiler Estrogen Receptor Signaling PCR Array (Qiagen).

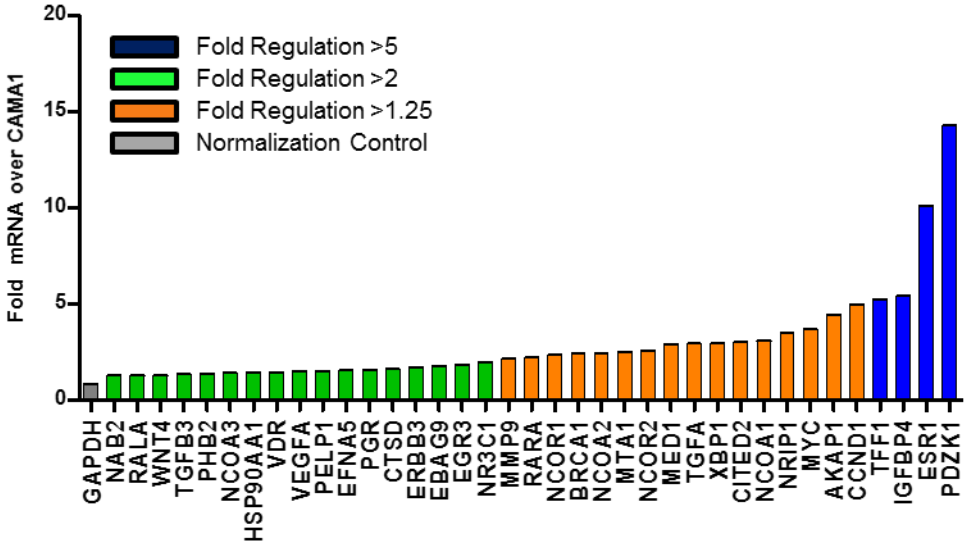

**Supplementary Figure 9. A,** CAMA1 cells were treated with 100 ng/mL FGF3 ± 1 μM INCB054828 in estrogen-free medium. After 15 days, plates were washed and stained with crystal violet and their imaging intensity was quantified as described in Methods. Representative images and quantification of the imaging intensity values as % of vehicle-treated controls are shown (**p<0.01 vs. controls, Fisher's t-test)**. B,** CAMA1 cells in identically treated parallel plates were treated for 6 h after which lysates were prepared and subjected to immunoblot analyses with the indicated antibodies. **C,** CAMA1 ± 1 μM INCB054828 were plated in estrogen-free medium and treated with 100 ng/mL FGF3 for 6 h. At this time, cells were harvested and RNA was prepared and analyzed for *THBS1, CCND1, CCL2* and *EGR3* mRNA changes by qRT-PCR. Each bar represents the mean transcript level ± SD (**p*<0.05, ***p*<0.01, ****p*<0.001 vs. CAMA1$^{GFP}$, Fisher's *t*-test).

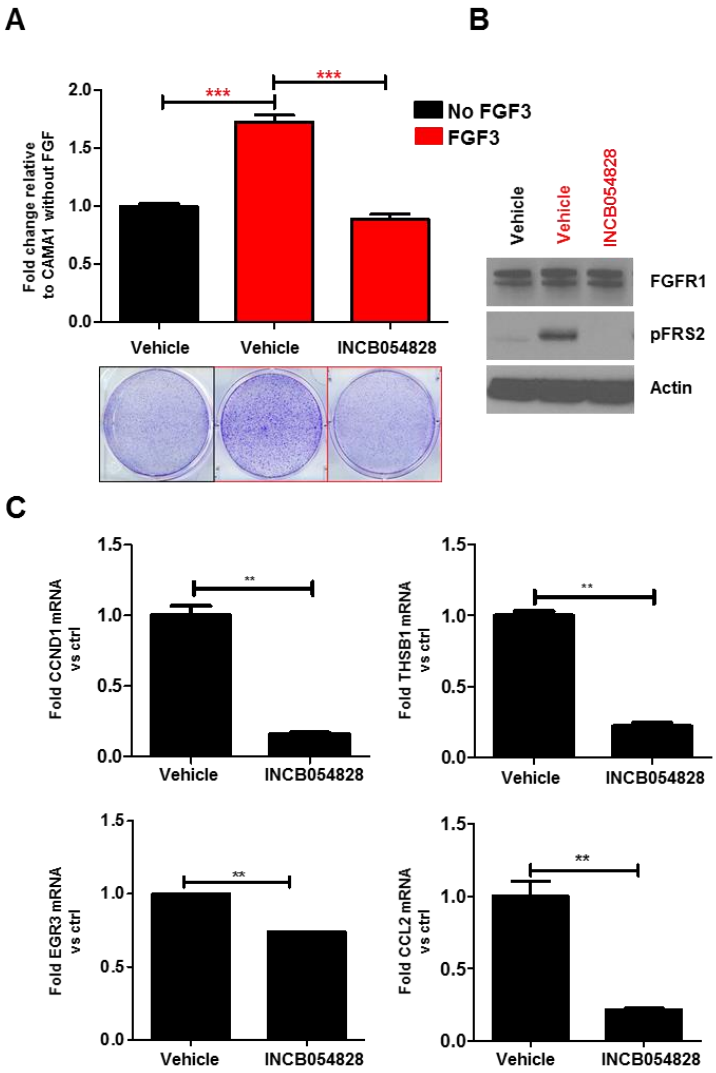

**Supplementary Figure 10. A,** ER+/HER2–/*FGFR1*-amplified T272 PDX tumors were established in female athymic nude mice supplemented with estrogen 8.5 mg/L in the drinking water. Once tumors reached ≥200 $mm^3$, mice were randomized to treatment with vehicle, fulvestrant (5 mg/kg/week), lucitanib (10 mg/kg/day), or both drugs for 5 weeks. Each data point represents the mean tumor volume in $mm^3$ ± SD (n=10 per arm; *p<0.05 vs. lucitanib; Fisher's t-test). **B-C** Weight of SCID/beige mice bearing T272 or TM00368 PDX tumors during treatment with vehicle, fulvestrant, lucitanib or the combination for a total of 7 and 3 weeks, respectively. The number of mice in each treatment arm is shown in parentheses. Each data point represents mean weight in grams ± SD.

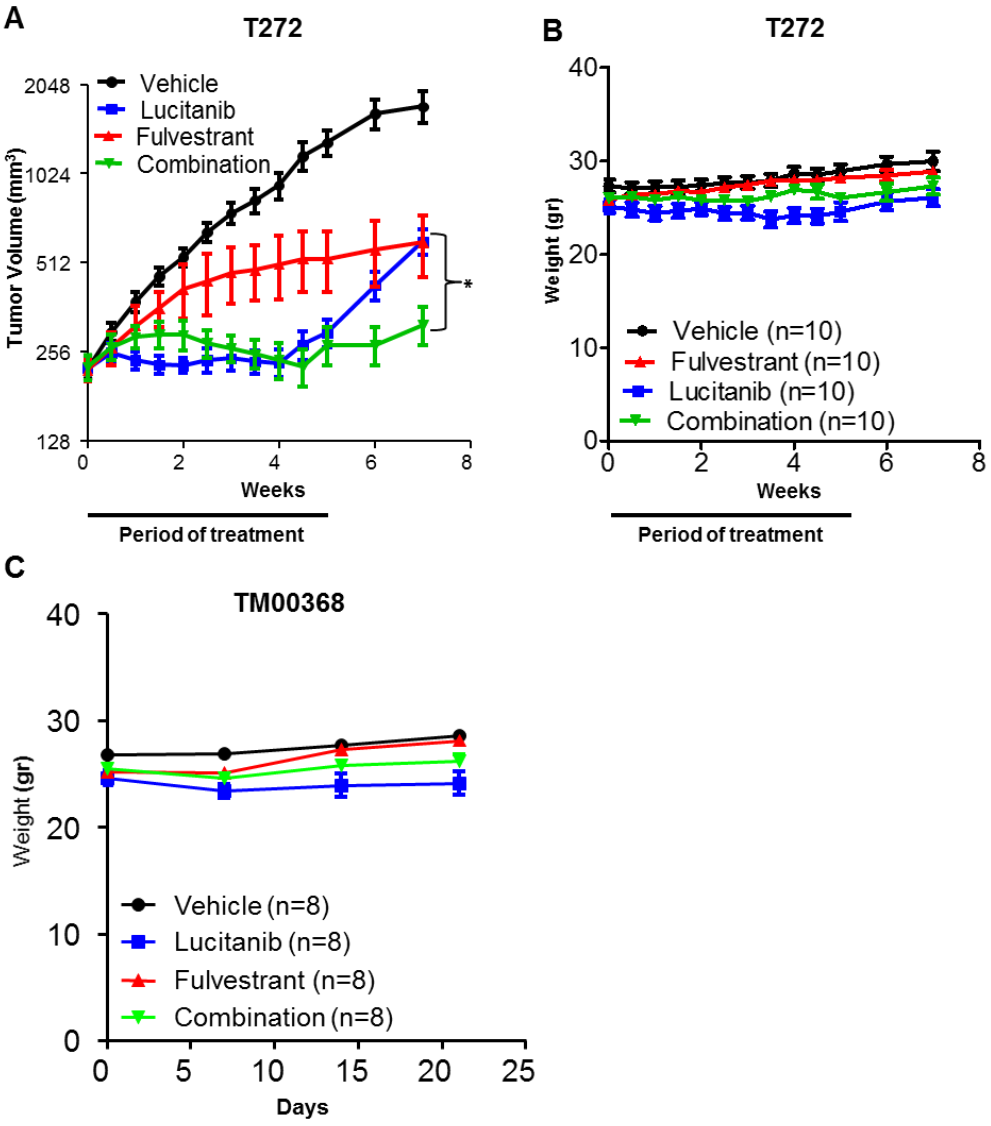

**Table S1**. Primer sequences used for ChIP-qPCR.

| Genomic Region | Fwd primer | Rev primer |
|---|---|---|
| 38477209:38479862 | TGGGTGTCTCTTGCTTCGTC | CATGATGTGTGCTGGAGGGT |
| 38477209:38479862 | AACCTTCAGCCCAGGAATCG | ATCTGCACAGTGGGTCACAG |
| 17271502:17274328 | GCCCCGCATAAAGAAAGCAG | AGCAAAAGCCGCAGTAGAGT |